Optimal Time Lags from Causal Prediction Model Help Stratify and Forecast Nervous System Pathology

Theodoros Bermperidis [1]*, Richa Rai [1], Jihye Ryu[4] and Elizabeth B Torres [1,2,3,*]

[1] Rutgers University, Psychology Department; tb642@psych.rutgers.edu
[1] Rutgers University, Psychology Department; rr708@psych.rutgers.edu
[2] Rutgers University Center for Cognitive Science (RUCCS); ebtorres@psych.rutgers.edu
[3] Computational Biomedicine Imaging and Modelling
[4] University of California Los Angeles, Neurosurgery Department; jihyeryu@mednet.ucla.edu
* Correspondence: ebtorres@psych.rutgers.edu; Tel.: +011-732-208-3158 (E.B.T.)

Received: date; Accepted: date; Published: date

Abstract

Traditional clinical approaches diagnose disorders of the nervous system using standardized observational criteria. Although aiming for homogeneity of symptoms, this method often results in highly heterogeneous disorders. A standing question thus is how to automatically stratify a given random cohort of the population, such that treatment can be better tailored to each cluster's symptoms, and severity of any given group forecasted to provide neuroprotective therapies. In this work we introduce new methods to automatically stratify a random cohort of the population composed of healthy controls of different ages and patients with different disorders of the nervous systems. Using a simple walking task and measuring micro-fluctuations in their biorhythmic motions, we show that gait is compromised in healthy aging and that in young FMR1 premutation carriers, gait forecasts, even by 15 years ahead, symptoms resembling those of elderly with Parkinson's disease. Our methods combine non-linear causal network connectivity analyses in the temporal and frequency domains with stochastic mapping, defining a new type of internal motor timings amenable to create personalized clinical interventions. We frame our results using the principle of reafference and operationalize them using causal prediction, thus renovating the theory of internal models for the study of neuromotor control.

Keywords: Granger causality; stochastic analysis; gait; network connectivity; Parkinson's disease; healthy aging; FMR1 premutation carriers

Introduction

Patients with Fragile-X Tremor Ataxia syndrome (FXTAS), patients with Parkinson's Disease (PPD) and patients in the broad spectrum of Autism (ASD) my all have motor issues detectable and tractable through gait patterns at different stages of their lifespan [1-10]. Generally, these disorders share some common genes [11-13], but their phenotypic features differ depending on the person's age and on the evolution of various epigenetic factors [1,14,15]. While the autistic patient may arrive at the diagnosis via Psychiatric/Psychological measures, devoid of motor criteria, it is highly probable that the PPD will do so through motor criteria from a movement disorders specialist in Neurology. In contrast, the FXTAS patient may receive an ASD diagnosis during childhood, when differences in communication and social interactions gain priority over motor issues [16,17] but then, later in life, as motor issues are exacerbated, they may gain the diagnosis of PPD. FMR1-premutation carriers may be considered neurotypical until later in adult life, when tremor, ataxia, and symptoms of parkinsonism become highly visible [18,19]. Indeed, the FMR1 CGG repeat length predicts motor dysfunction [20] of the type that PPD have much later in life.

We know that motor activity reveals that aging with Autism greatly departs from typical aging [21] despite whether the person is or is not on psychotropic medications [22]. We are also aware that parkinsonism, typically associated with human aging [3,23], is prevalent in Autistic adults [24]. Indeed, the rate of parkinsonism in the general population aged 65–70 has been estimated at 0.9 % [23], compared to 20 % in ASD aged after 39 [24], when excess involuntary motions at rest have been quantified [21,25].

Parkinsonism in FMR1-premutation carriers may be indistinguishable from PD [26]. And Fragile-X syndrome (FXS) has high penetrance in Autism [27] with genetic overlap across Parkinson, Ataxias, ASD and FXTAS [11]. This points to a common pool of genes affecting both neurodevelopment and neurodegeneration, perhaps providing a new path to pre-emptively offer neuroprotective motor-sensory-based accommodations in early neurodevelopment gone astray [11]. Given the high heterogeneity in their manifestations and the asynchronous nature of their developing severities, how could we automatically stratify a random draw of the population containing a mixture of these disorders?

Gait studies integrated with wearable sensors in natural activities have been very useful to ascertain various aspects of these phenotypes [19,28-30], but population statistics employed in these analyses are not personalized. They primarily focus on descriptive summary statistics from a priori assumed distributions, a procedure that incurs in loss of gross data [31]. Further, owing to anatomical disparities confounding gait parameters, we need scaling methods that standardize outcomes and provide proper similarity metrics to compare across different subtypes of a given disorder. There is room to examine individual motor fluctuations within the context of dynamic network analyses and causal prediction [32]. Here we integrate causal and non-causal network connectivity analytics to examine self-emergent patterns from standardized micro-movement spikes derived from gait-kinematics. We discuss our results within a new unifying framework to study disorders of the nervous systems across different diagnoses of disparate clinical criteria and yet, converging functional phenotypes.

Results

Granger causality (GC) is a mathematical concept that allows us to quantify the causal effect of a stochastic process A on a second stochastic process B. It compares the prediction error of a dynamic model that predicts the evolution of B without the presence of A with the error of a prediction model that includes both A and B. If the inclusion of A improves the prediction, we say that A causally predicts B (A➔B) and we can assess the degree to which this is determined by the method of choice. Our approach to modeling and calculating the Granger causality assumes models with a single internal delay. This allows us to find, within a particular range, the internal delay that maximizes the causality from A to B. To implement our methods using time series data from a grid of 23 sensors collecting bodily orientations as the person walks, we first extract the angular speed time series (rad/s) over the span of 3-min walks. We then, build a data type that we have created the micromovements spikes (MMS [33]) which extracts the moment-to-moment fluctuations in the signal's amplitude provided by the peaks, and the fluctuations in inter-peak interval timings. This data derived from the sensors is unitless as it is standardized to characterize the dynamic behavior of motion by scaling out anatomical differences. This standardization of the data also enables us to compare the stochastic signatures of these participants' motions across a random draw of the population, while considering different ages and different clinical genotypes and phenotypes. As we keep the indexes into the original physical unit ranges, we can further estimate cross-population scales and boundaries for each parameter of interest.

Upon standardization, we apply our technique between each directed pair of MMS time series across all 23 nodes corresponding to different joints across the full body. The maximum outwards GC of each node towards the rest of the body for the average GC-directed network of each group revealed marked differences from group to group. Furthermore, the average Optimal Lag network of maximum lags from a node to the rest of the body, assuming that the MMS series of that node, is the causal stochastic process, also revealed fundamental differences on timing across the different ages and nervous systems' disorders. We detailed them below:

Granger-Causal Networks Reveal Age-Dependent Gait Differences in Typical Controls

As age increases in healthy participants, we see fundamental differences emerge in the patterns of GC prediction between their upper and lower body. The relative causal connectivity between upper to lower body is higher in elderly participants than in young controls. This can be appreciated in Figure 1A using an anthropomorphic interconnected network representation of the full body using the 23 nodes. The size of the node is proportional to the GC out degree value of that node as it connects to all other nodes. Furthermore, elderly control participants have in general lower optimal lag times of the lower extremities (*p=0.0293, t-test*) suggesting an overall slowdown in information transmission and feedback between upper and lower extremities. Often, patterns such as bradykinesia and loss of gait control in pathologies of the nervous system are shown. Yet, here we observe them as a part of the natural aging process in this cross-sectional cohort of healthy controls. We use a colormap representation to indicate the lag values in Figure 1A, whereas in Figure 1B, we provide the empirical frequency histograms of the interpeak interval timings of the MMS. The corresponding physical times expressed in seconds distribute according to the continuous Gamma family of probability distributions, optimally fit to the empirical data, in a maximum likelihood estimation (MLE) sense. These patterns are depicted for the healthy controls in Figure 1B (top panels.)

FMR1-Carriers are Different from Controls of Comparable Age and from PPD

Premutation carriers of the FMR1 gene show a significant decrease in GC connectivity across the body in relation to the young controls of comparable age (*p=0.0061; t-test*) This is depicted in Figure 1A along with fundamental differences in the patterns of optimal lags, which are abnormally lower than controls (*p=2.7160e-04; t-test*). This reduction in optimal lag values in the premutation carriers is accompanied by a reduction in their timing variability that resembles (and perhaps forecasts) the type of reduction in variability observed in the PPD. The latter shows a significant reduction in GC across the body relative to the elderly controls (*p=0.0021; t-test*). This is particularly the case in the torso, with lower lags in the lower body, when we compare them to the elderly controls. Figure 1C summarizes the statistics of the timing. This parameter space reveals healthy patterns of timing variability in the controls *vs.* atypically lower variability patterns in the premutation carriers and the PPD.

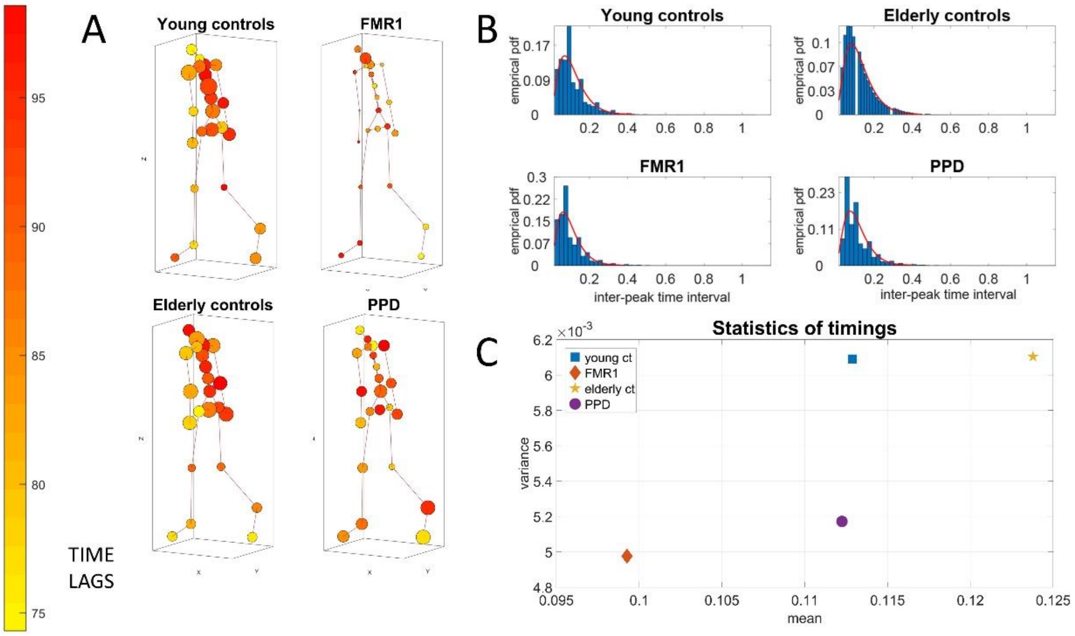

Figure 1: **GC Optimal Lag Maps and timing information.** Anthropomorphic network representation of human walking patterns. The nodes' size is proportional to the number of outgoing links connected to the other nodes in the network (out degree) of the average GC network. The color of the nodes is the maximum optimal lag response of a node with the rest of the body for the average Lag Response network. A unit of one lag refers to the distance in time between two peaks. The actual physical time between the two peaks can vary. The frequency histograms depict the distribution of the inter-peak timings for each group. The empirical distributions are well fitted by the gamma family of distributions. For the young controls, the average inter-peak timing is 0.1129 seconds with a std of 0.0780. For the elderly controls, 0.1238 with a std of 0.0781. For the FMR1 carriers, 0.0993 with a std of 0.0705. For the PPDs, 0.1122 with a std of 0.0719.

Prevelance of causal feedback loops is much higher in controls groups

An important concept in the theory of neuromotor control, first introduced by von Holst and Mittelstaedt in 1950, is known as the principle of reafference [34]. Every time a motor movement is to be initiated, a motor signal is sent to the periphery to perform a certain movement through the efferent nerves, which is called efference. Similarly, the sensory input coming from the periphery towards the Central Nervous System (CNS) is called afference. The afference consists of two components. The first component is called exo-afference and is the afferent input generated from the environment. The second component is called endo-afference, which is the sensory input self-generated from the body's own actions. We discovered that during complex actions, the endo-afference is separable into intended segments (under voluntary control), and incidental segments (occurring spontaneously and largely beneath awareness [35].) Because of its internal origins and its relation to movements, the latter is known as kinesthetic reafference, though it also includes pain and temperature afference from the corresponding fibers at the periphery. According to the principle of reafference, every time a movement is initiated by sending information to the motor system, a copy of the signal is created, called the efferent copy or corollary discharge, and is sent to the CNS to inform of the impending movement. This enables the CNS to distinguish sensory signals stemming from external environmental factors, from sensory signals coming from the body's own actions. The efference copy is provided as input to a forward internal model to predict the sensory consequences of the motor action to be initiated. Comparing the predicted movement with the actual movement is precisely what allows the CNS to recognize its own actions and at a higher cognitive level, form a sense of self. In the internal models of neuromotor control, the intended consequences from voluntary acts can be evaluated using the principle of reafference [36,37]. A non-trivial extension of this idea is to include, in addition to consequences from voluntary actions, the unintended consequences from those incidental actions that occur spontaneously, without instructions or precise targets. This idea has been proposed and investigated by our group, to define different levels of volition [35,38-40], and proposed as a fundamental ingredient of the more general concept of motor agency.

The principle of reafference has been a source of inspiration for decades in biology, cognitive science, vision, neuromotor control and robotics, and attempts to model it fall usually within the realm of control theory and dynamical systems [41-44]. Our approach to operationalize this principle does not assume a particular deterministic feedforward model. It rather assumes stochastic dynamic models for each body node and for pairs of body nodes. If the principle of reafference implies the presence of feedback loops between the CNS and the periphery, the fact that information is carried along efferent and afferent pathways and processed in various organs of the CNS (e.g. the cerebellum [36]) implies that it is not an instantaneous process, but it is characterized by some internal timing. In fact, timing is important to accurately predict the consequences of one's actions, coordinating such actions in space and time. Timing plays a central role in agency, leading to a sense of action ownership and self-awareness. Hence, the causal analytics, being sensitive to the choice of timing of the model, can be used to estimate the actual motor timings in the nervous system.

But how exactly can we detect the presence or not of a feedback loop between two nodes? Once again, the answer can be found in one of Granger's definitions in his original paper [45]. Following the formal definition of causality, he proceeds to define feedback. According to the definition, if A and B are two stochastic processes, and A causes B in the Granger sense, but also B causes A in the Granger sense, *i.e.*, causality occurs in both directions, then that implies the presence of a feedback loop between the two processes. Then, simply checking for each undirected pair of body nodes, we can check whether the causal connectivity graph that we derived earlier exhibits causality in both directions. Then, we can determine whether there is a feedback loop between the nodes, within the accuracy of our model and the choice of timing.

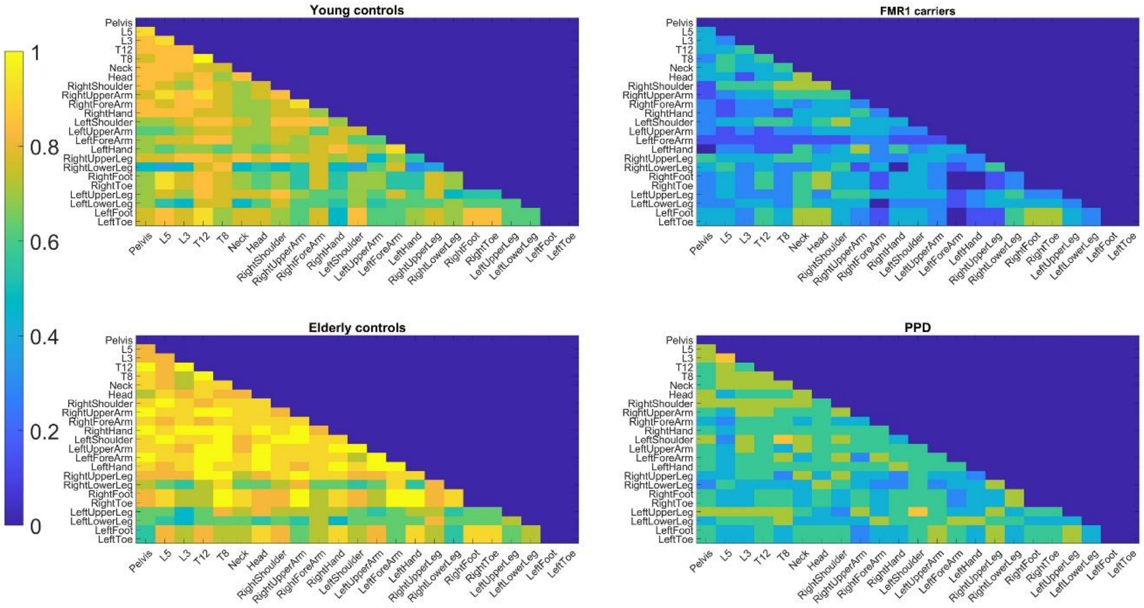

Figure 2: **Feedback loops differ across groups**. For each group, the figures show the percentage of subjects within the group for whom a feedback loop was detected between each pair of body nodes.

Addressing Granger's notion of feedback (up to our limited assumption of an autoregressive model explained in the Materials and Methods Figure *14*) provides the results depicted in Figure 2. Once again, the healthy controls show (cross sectionally) the effect of natural aging on the feedback patterns that we take pairwise across these 23 nodes of the body. Consistent with the Figure 1A summarizing the group patterns (in one direction A➔B), we see the patterns of feedback loops across each group, detected when including B➔A and obtaining GC in both directions. Young healthy controls have a more distributed pattern across the body, in contrast to elderly controls, who show a diminished pattern in the lower extremities accompanied by an abnormally higher feedback-loop pattern across the upper extremities, perhaps compensating for their lacking in the lower extremities. This decrease in feedback loops generalizes across all bodily nodes in PPD, but interestingly, the decrease is even more evident in the FMR1 premutation carriers, closer in age to the healthy young controls. At such a young age compared to the PPD, these patterns in the FMR1 premutation carriers forecast trouble on the horizon, of the type that elderly PPD eventually show.

Identification of Different Groups' Subtypes

One of the current challenges in data-driven analyses is to automatically identify self-emerging subtypes of a disorder on a spectrum, as patterns stratify to form clusters of data points across a given scatter. We here address this automatic stratification of a random draw of the population composed of different types of patients and ages using various parameter spaces derived from the stochastic patterns of the gross data that is often thrown away or smoothed out through grand averaging.

For each participant, we calculated the trajectory of the Center of Mass of the lower body in 3D space and we extracted the MMS series from the Euclidean norm of the position time series. Upon obtaining the standardized (scaled) speed amplitudes, we obtained the peaks and calculated the empirical distributions of the inter-peak-interval timings of these MMS series. We noted the presence of multiple modes in the frequency histograms and performed the Hartigan Dip test of unimodality [46]. We performed this statistical test both on the patterns from each participant separately and pooling the data across participants for each group. For the latter, we did so after concatenating the MMS series data of all subjects within a group. The Hartigan Dip Unimodality test per group showed that for all groups the total empirical distributions fail the unimodality test. All groups distributed bimodally, yet how the modes grouped had specific patterns particular to each group. This is depicted in Figure 3.

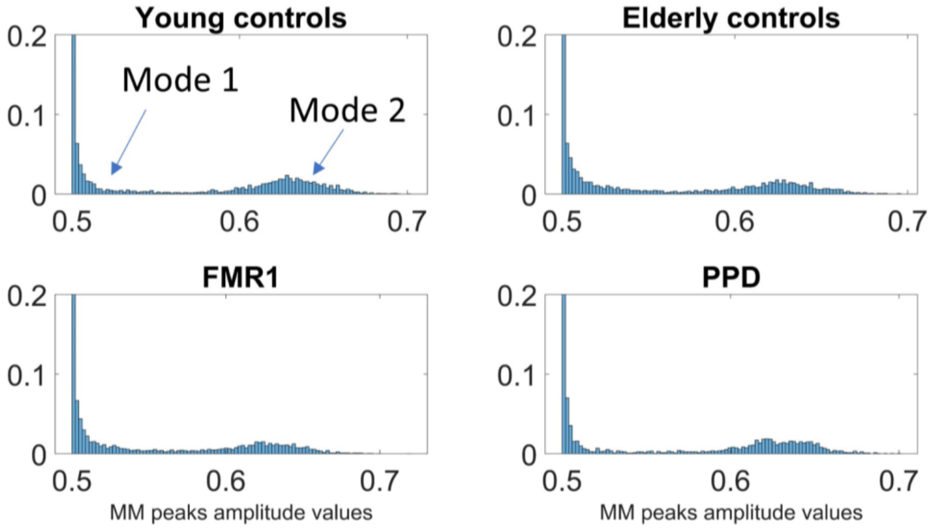

Figure 3: **Non-unimodal distributions of MMS from peak angular speed amplitudes differentiate groups**. Different modes are specific to each cohort, mode 1 exponential and mode 2 Gaussian, with different dispersions and percentages of points in each mode.

The first mode with lower values of the standardized MMS peaks amplitude was well fit by an exponential distribution, whereas the second mode was well fit by a Gaussian distribution that had the lowest dispersion in healthy young controls. In elderly controls, the percentage of points in the exponential mode increased, and so did in FMR1 premutation carriers (closer in age to the young controls) and the PPD, with the latter showing distribution patterns comparable to the carriers. To see this, for each participant, we found in which mode the MMS activity was highest and calculated the percentages of participants per group with the highest activity in each mode. Most young and elderly controls have the highest MMS activity in the Gaussian mode. FMR1 carriers and PPDs have higher prevalence of activity in the exponential mode (Figure 4.)

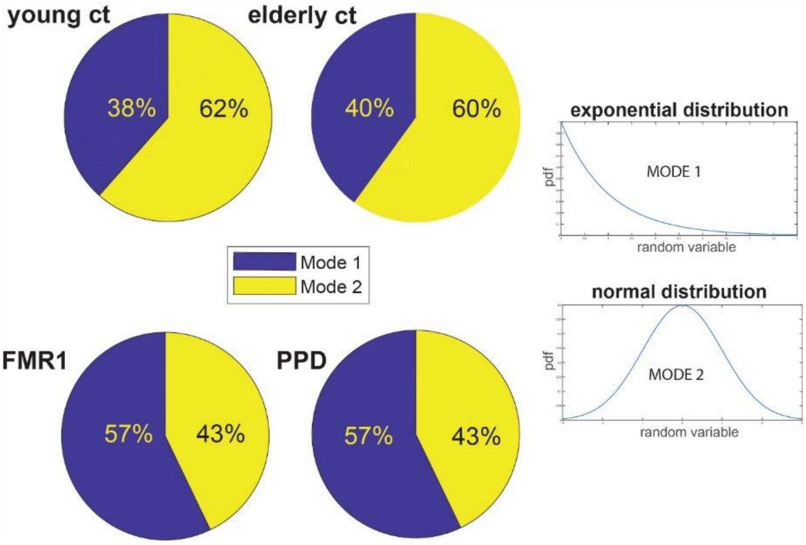

Figure 4: **Percentages of distribution's modes varies across groups** with lowest Exponential mode in young controls and highest in FMR1 carriers and PPD. Gaussian mode is highest in young controls and elderly controls and comparable between PPD (higher) and FMR1-carriers.

These patterns motivated a parameter space whereby we represent points as triplets -points in a three-dimensional space, with coordinates representing the % of Mode 1 (exponential), the Dip value from the Hartigan's Dip Unimodality test, and a scalar, giving the speed to frequency ratio (we discuss below the motivation for using this ratio.) We then performed k-means clustering analyses on the scatter of points from each group, to identify potential subtypes of activity in each cohort of participants.

Figure 5 depicts the results (under the Euclidean distance metric; note that using the first mode in this representation is sufficient, as the second mode percentages are complementary, *i.e.,* the sum of percentages add to unit). Here the young controls have 3 clusters, and the other groups show 2 clusters (represented proportional to the size of the marker.)

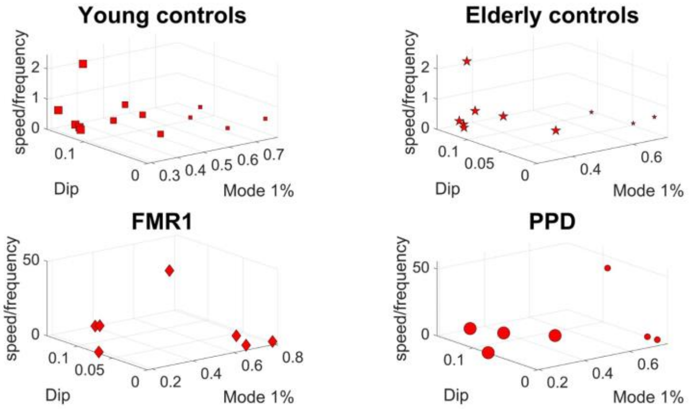

Figure 5: Subgroups within each group revealed by group's clusters. The clusters for each group using the k-means clustering algorithm with 3 for young controls and 2 for each of the other groups. Subtypes of activity emerge for all groups. The empirical distributions for the MMS of the norm of the lower body COM 3D position data series for the 4 groups are bimodal for all 4 groups.

We identified 3 sub-types for the young controls group and 2 sub-types for the elderly controls. There is a clear negative correlation between higher dips and lower first mode activity. The FMR1 carrier group has two subtypes. The first subtype has high first mode activity and low dip and the second subtype has low first mode activity and high dip. A similar subtyping pattern is observed for the PD group. The results can be appreciated in Figure 5, where the size of the marker denotes the group within each cohort.

Groups Differ Relative to Young Controls within a Parameter Space from the Data Stochastic Features

The above results motivated us to quantify the departure of each group from the young controls (as an ideal, normative state of motor control.) To that end, since the lower body and the pelvis play a crucial role in gait control, we first characterized the patterns of fluctuation in the motions of the pelvic area and upper leg nodes) by fitting the continuous Gamma family of probability distributions as the optimal family in an MLE sense. Through this process, we obtained the scale parameter, which is also the noise to signal ratio (NSR.) We obtained the average NSR and computed skewness of the MMS series of the pelvic area for each subject. We also obtained the GC network asymmetry for each subject (See Methods). This paramer space is shown in Figure 6 across all three comparisons.Two sample *t-tests*, showed that young controls differ from elderly controls in mean skewness (with bortherline significance, *p-value=0.096* , *confidence interval=[0.0465, 0.0299]*). They also differ from PPDs, signficantly at the *0.05 alpha level*, in mean pelvic NSR (*p-value=0.0193* , *confidence interval=[-0.047, -0.00047187])*. Finally, they differ significantly from FMR1 carriers in assymetry *(p-value=0.0107, confidence interval=[-0.3386, -0.051])*. In each plot, we fitted surfaces over the data samples for the young controls to help visualize the differences and localize each cluster shifting across the parameter space relative to this normative surface.

Notice in Figure 6 that FMR1 and PPD depart similarly from the normative surface of young controls, while the elderly controls occupy a different location in this parameter space.

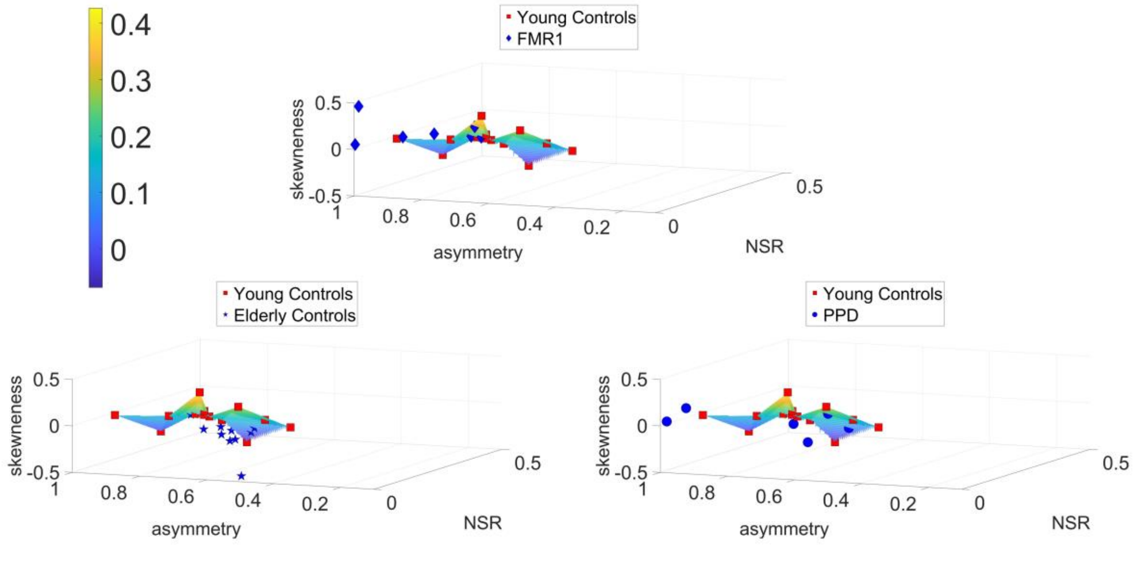

Figure 6: Parameter space reveal differences across groups. NSR, GC network asymmetry and average Skewness are used to build a parameter space showing departure from young controls scatter fitted by a surface. Scatters from the FMR1carriers, the elderly controls and the PPD largely depart from young controls' surface. Color bar reflects skewness range of values.

To examine temporal information within the efference-reafference framework, we calculated for each undirected pair of angular speed MMS time series (*i.e.*, the full time series, not only the peaks) the coupling frequency for which the cross-coherence is maximized. To that end, we found the average of all cross-coherence outputs of a node's MMS series with all the other MMS series nodes in the network (see Supplementary Materials). The time between two MMS is essentially a form of inter-spike interval timing for the information flow crossing each body node. Therefore, we average for each group the inter-spike times of each node and compare the rate of putative afferent (incoming) and efferent (outgoing) activity. Figure 7 shows the patterns from a series of t-tests between the timings using every possible combination of the two groups for each node. Zero entries mean that the t-test was not significant, non-zero entries show the average differences between the mean times for each group.

We note that FMR1 carriers exhibit much higher inter-peak timings in the thoracic area and the lower leg area than the PPD subjects. Both young and elderly controls seem to have much higher inter-peak timings in the left arm and hand than PPD patients. Interestingly, FMR1 carriers seem to depart further away in their timing profiles from elderly controls than elderly do from the young controls. This suggests that the healthy aging process may not significantly alter the afferent or efferent rate of activity in any specific area of the body, despite increasing the inter-peak interval timing (on average) for the entire body. As we saw earlier (Figure 1) these consistent patterns perhaps hint that aging may be spatially non-specific with regards to the rate of activity. On the other hand, aging seems to decrease the efferent and afferent activity as well as increase the internal motor timings of the system.

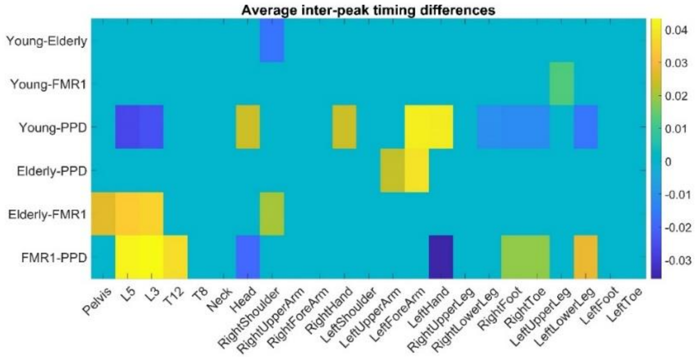

Figure 7: The average differences in inter-peak timings (seconds) taken for each group across all nodes, reveal separation between groups. A difference of zero (cyan color) indicates no significant difference (*p=0.05*).

Analyses across the 23 nodes are visualized as an anthropomorphic interconnected network representation in Figure 8A. The figure shows the average inter-peak interval times as the color of the node. The average cross-coherence output of each node's MMS series is proportional to the size of the node. We appreciate differences between the size of the nodes for the different groups, hence reflecting differences in the maximum coupling frequencies. Methods Figure 13 shows the analytical pipeline to obtain pairwise cross-coherence, along maximal values of the coupling and corresponding phase lags and frequencies employed in the derivation of relevant parameter spaces.

For each subject, we calculated the average speed of the COM of the lower body, as well as the average frequency of the speed time series. We did so, to study how the kinematics of a subject relate to the stochastic signatures of the MMS activity. For all groups, except the FMR1 group the speed generally increases with respect to the frequency while for the FMR1 carriers the speed decreases. This is depicted in Figure 8B.

The speed is in m/s and frequency is in Hz, or 1/s. Therefore, speed over frequency has unit of meters. Behind this unit analysis, an important biomechanical concept is "hidden". Due to the periodic nature of gait, frequency expresses the number of walking cycles or strides per unit time. Speed on the other hand, is the average distance traveled by the center of mass of the lower body per unit time. Distance over time divided by number of walking cycles over time gives us the distance traveled *per* stride. Revisiting Figure 5, we observe that the third dimension, which is speed over frequency does not really differ between participants of each group. This indicates that cumulative distance per stride could be an invariant quantity by which we could characterize each group. Figure 8C shows the different patterns of cumulative distance per stride across participants. We note here that the larger the amount of high frequency jitter in the MMS, the larger the accumulation counting towards the stride length. As such, some participants in the PPD and FMR1 carriers (both of which develop tremor eventually) already show signs of this dysregulation of involuntary jitter in the walking patterns.

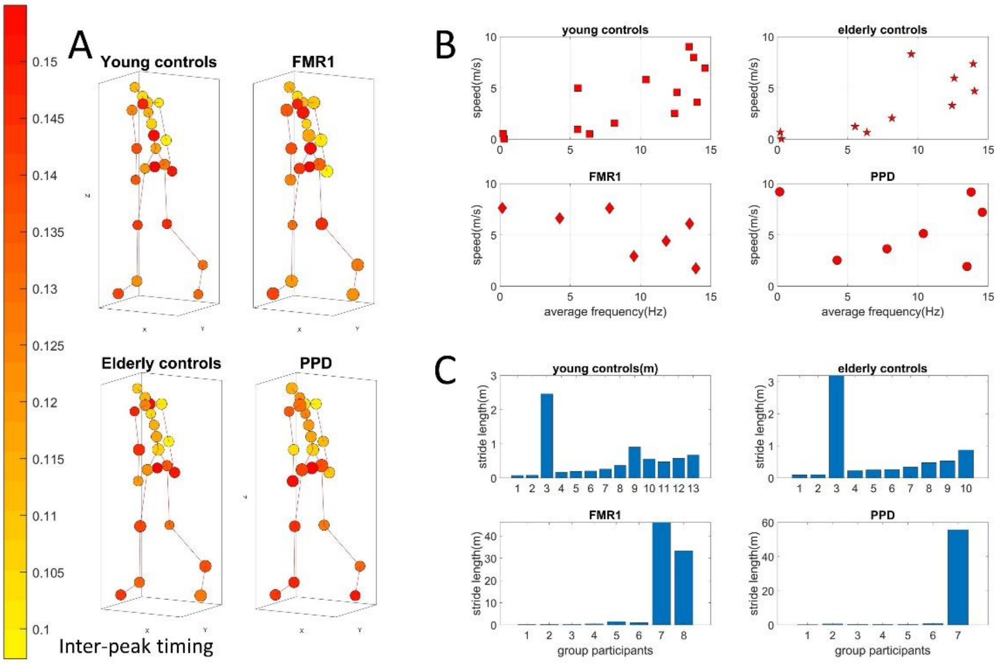

Figure 8: Stride-length differences from speed to frequency ratio obtained from the center of mass trajectories, separate healthy aging from nervous systems disorders. (A) Network representation in anthropomorphic avatar form. The size of the nodes is proportional to the maximum coupling frequency (the one that maximizes cross-coherence) of a node with the rest of the body and the color of the nodes is the average time distance (s) between two MMS peaks. (B) Parameter space comparing speed vs. frequency. Focusing on the trajectory of the center of mass of the lower body, mean speed over mean frequency of the speed time series has a positive upward trend for healthy controls. This contrasts to a negative trend in FMR1-carriers and variable trends in PPD. (C) Both types of trends and variations span a range of values across both dimensions with stride length periodically accumulated differing across groups.

A form of Noise Cancellation with Possible Therapeutic Value

The value of examining feedback loops, timing, and stochastic signatures across the population, can be better appreciated within the context of noise cancellation. Noise cancellation helps engineer solutions and build accommodations for PPD and other disorders of the nervous systems with tremor-related signals. Along those lines, here we investigated how removing different frequency bands from the angular speeds of the PPD affected the network dynamics. We tried different combinations of low and high limits for the frequency stop band to filter out tremor components (as reported by the literature [47] and performed *t-tests* between the resulting group and the elderly or young control groups for each body node. Then, we measured the number of nodes in which the two groups differed significantly in the NSR. We then interpolated a surface on the parameter identification data.

We report that the optimal tremor removal when comparing to the healthy young controls group is for frequencies above 19 Hz, while the optimal tremor removal when comparing to the old controls groups is for frequency band with low limits near 10 Hz. Figure 9 shows these differences.

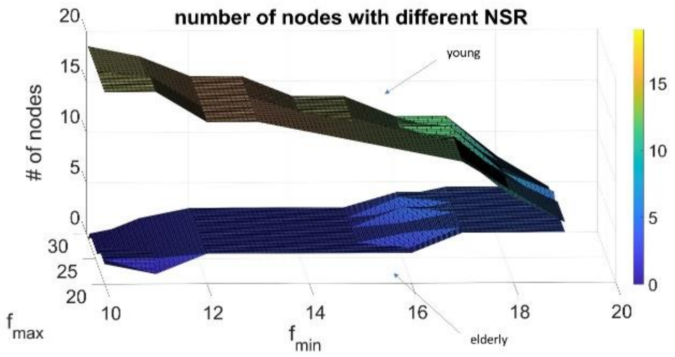

Figure 9: Noise cancellation by systematic frequency removal in young *vs.* elderly participants. The two surface plots show how after removing a component of tremor from the PPD by using band stop filtering of the angular velocity for different choices of frequency, the resulting body node networks is comparable to the NSR dimension of the young and elderly controls groups. The color bar reflects the number of nodes with different NSR that results from the noise cancellation.

MMS Amplitude and Timings are Not Independent

Lastly, to further understand the spatio-temporal characteristics of the MMS signal derived from the angular speed, we calculated the empirical joint distributions of the MMS inter-peak-interval times and the distributions of the MMS amplitude (peak values). We asked if they were independent. The results are shown in Figure 10. The complex patterns that emerge indicate that assuming independence between the rate of MMS activity and the MMS values is only a first approximation to a more complex mechanism that needs to be further investigated.

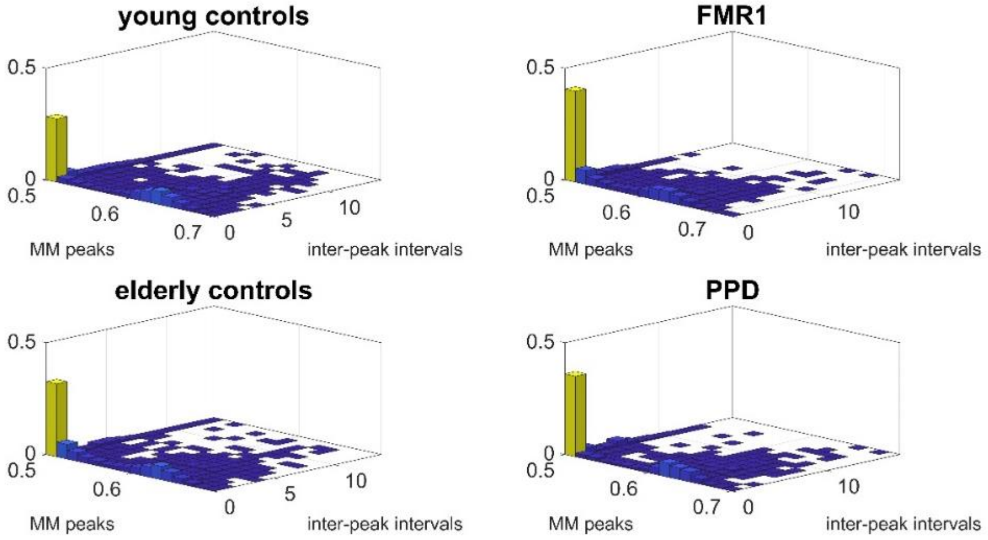

Figure 10: Joint empirical distribution of MMS peak values and inter-peak-interval times.

Discussion

This study explored walking activity in the context of natural aging and well-established neurological conditions found in PPD and FMR1 premutation carriers. We aimed at examining the patterns of variability from kinematic parameters that would automatically stratify this random draw of the population. Furthermore, we explored the movement trajectories of 23 joints across the body, with the purpose of deriving information related to internal temporal lags in information flow. To that end, we framed our problem within the context of causal prediction models of outgoing efferent and incoming reafference information flow, derived from time series of micro-movement spikes. We distinguish these internal time lags from external movement times modelled a priori in biomechanics and robotics. Such trajectories' time profiles are often modelled using the equations of motions to study human movements' trajectories within some optimization framework (*e.g.*, optimal control models such as minimum jerk [48] minimum torque rate [49], minimum energy [50], among others.) Temporal dynamics have been modelled as well in studies of motor control, within the frameworks of stochastic optimal control and reinforcement learning [51,52]. In human and animal psychophysics studies associated with reaction times, temporal information is often derived from computer mouse-clicks or lever presses, respectively, within the context of perceptual learning, decision making and other tasks in the cognitive domain [53-56]. We also distinguish the notion of internal temporal lags reported here from such studies.

To better appreciate the difference between the internal time lags examined here and those from biomechanics, or from reaction time tasks, we invite the reader to distinguish between a person-centered perspective, *i.e.*, obtained in personalized and objective manner, and an observer-centered perspective. The latter makes a statement about the observer's appreciation of actions' trajectory timing under some a priori defined population statistics, or grand averaging parametric model. It also imposes a theoretical classical mechanical time-dependent model that is incongruent with empirical data. Empirical studies show that the geometry and the forces characterizing motion trajectories are separable, *i.e.* unlike in inanimate rigid bodies in motion, in biological bodies with nervous systems, the trajectory's temporal dynamics depend on the level of intent that cortical neurons plan and update online (e.g. [57] *vs*. [38,58-61]). The temporal dynamics of motion trajectories also depend on subcortical regions thought to specify the rate of change in bodily configurations, as the body transitions from one configuration to the next [62,63], and we can model it and study it in PDP [59,61]. In contrast to these centrally defined timings, internal time lags examined here, aim at characterizing temporal dynamics from the efferent and reafferent flow of information across the person's body, at the periphery. This characterization is done empirically, by estimating the person's stochastic signatures from the individual fluctuations in the signals' peak amplitudes and inter-peak-intervals' timings within the framework of causal prediction in time series forecasting analyses [32,64] and augmenting von Holst's principle of reafference to include non-voluntary aspects of actions' consequences into the feedback that the brain receives from internally self-generated actions.

We here define motor timing as the internal timing for which there is a maximal causal relationship between two neuromotor processes. The internal timing is a stochastic quantity defined as the random distance in time between two micro-movement-spike peaks. This is different from the biomechanical physical time of a motor event, measured by an observer-centered external clock device describing the motion trajectories and / or the decision times of cognitive tasks. As mentioned, in the former we find families of models that derive temporal dynamics using classical equations of motion (originally derived for inanimate, rigid bodies). In the latter we find reaction times associated with decisions and cognitive performance from animate, autonomous agents.

While models of biomechanical times cannot account for empirical results in motor control pointing at a fundamental separation between intended and unintended actions, animal and human models of reaction times highlight the subjective nature of time perception during reaction tasks in mammals [65] aiming for a general population statement, rather than for an individualized characterization of the temporal dynamics phenomena. In the present study, we aimed for a person-centered approach that also led to self-emerging stratification of the cohort. Instead of a priori assuming a given distribution to characterize the moment-by-moment fluctuations in the walking parameters, we let the data drive our exploration, revealing maximally informative parameter spaces that automatically separated our cohort into clusters.

Indeed, proper parameter spaces allowed us the separate natural aging, PPD and FMR1 premutation carrier syndrome from the baseline of motor activity in young controls. Of particular interest was the finding that in natural aging, the lower extremities are compromised, leading to a reduction in the causal prediction of lower body by upper body extremities. This is accompanied by a lengthening of the optimal time lags describing information flow derived from fluctuations in movements. Indeed, the naturally aging person tends to have less communication flow and higher noise-to-signal ratio than the younger controls. This result was clearly expressed in lower feedback from the legs and feet to the upper body. The peripheral flow of information appeared to be severely compromised in the elderly PPD and surprisingly so in much younger FMR1 carriers.

The moment-by-moment fluctuations in the peak amplitudes of the MMS offered new ways to stratify this random draw of the population and clearly distinguish each subgroup in relation to young controls. Of particular interest here is the multimodal nature of the peaks' distributions revealing a prevalence of the exponential family that increased with natural aging and was much more prominent in FMR1 carriers and PPD participants. This result highlights the random, memoryless nature of the fluctuations in these groups. It also explains the marked reduction in causal prediction of upper-to-lower body and the lack of feedback from lower to upper body found in the FMR1 carriers and in the PPD participants. Importantly, the person-centered approach used in this work was amenable to reveal within each group (young, elderly, PPD and FMR1 carrier) different subtypes according to the center of position derived from the lower body kinematics. We used these results to further derive parameter spaces that combined asymmetry in Granger Causality, noise-to-signal ratio, and distribution skewness to express and to differentiate each group in relation to young controls. Pair-wise differentiation and patterns were also revealed by the inter-peak timing analyses of the trunk, arms, and legs regions, with different trends in natural aging *vs.* aging with a nervous system pathology.

The results from this study are amenable to build diagnostic tools using parameter spaces derived from a simple walking task. Furthermore, the work offers a unifying framework to help predict the early appearance of large departure from normative ranges in young controls, both for normal aging and for young participants who are FMR1 carriers. This is important, given the high penetrance of FX-related syndrome in other neurological conditions across the lifespan. Among these are ASD, FXTAS and PD. The methods described here offer a new way to detect these gait problems 15-20 years ahead of their clinical onset and as such, could help advance neuroprotective intervention models.

While our analysis uncovered the relationship and similarity between PPD and FMR1 carrier syndrome, it also sheds light to the process of natural aging and how individuals with PPD age differently from neurotypicals. Our results indicate that in elderly controls, there is higher overall causal connectivity in the lower body compared to young controls. It is possible that this is related to the degeneration of motor functions in the lower body which comes naturally with aging. To preserve balance and avoid falls, the nervous system will incur in higher cognitive load. As such, natural walking, a process that is rather automatic in young people becomes cognitively effortful and requires higher concentration as we age. This higher cognitive (central) demand may be reflected in the lower body connectivity at the periphery, and poorer lower-to-upper feedback patterns found in the elderly participants.

The results also reveal fundamental differences between PPD and much younger FMR1 carriers, who nevertheless, also showed a marked reduction in feedback from the lower to the upper extremities. These two subgroups were far apart in age, yet both revealed large departure from young controls and timing patterns closer to those of the elderly controls.

PPDs, show not only a significant increase in lower-body connectivity, but also a marked reduction in upper-body connectivity. This pattern suggests that the degeneration of motor control in PPD is not limited to the lower body, but that in fact, it is a disease that affects the motor system in a general and systemic way. A higher cognitive load is required to control the lower body which as a side effect may result in poor connectivity in the upper body, and poor systemic coordination with impaired kinesthetic sensory feedback. Interestingly, when comparing how the inter-peak timings of each body node differ between groups, we can conclude that in that sense, the elderly controls and the FMR1 carriers are almost identical to young controls. On the other hand, PPDs have significant different inter-peak intervals' timings than young controls. This not only shows the departure of PPD from natural aging, but also shows that despite the Parkinsonian symptoms of FMR1 syndrome, the latter is still a fundamentally different condition than PPD.

Finally, as a potential actionable application of the present work to mitigate the high levels of noise found in the walking patterns of PPD and FMR1 carriers, we used the relationship that Granger's causal prediction methods offer between frequency and time domains. Inspired by Granger's approach, we developed a network-connectivity based model of noise cancellation. Specifically, we systematically removed frequencies reportedly associated with tremor in the literature [47] and quantified the outcomes of this systematic removal on the noise portrait derived from the time series analyses of angular speed peaks of walking patterns. We found differing ranges of optimal tremor removal relative to healthy young *vs.* elderly controls group. The former reveal optimal ranges for frequencies above 19 Hz, while the latter showed frequency band with lower limits, near 10 Hz. More exploration of these aspects of noise cancellation are warranted, yet using the present approach exploring internal optimal time lags within the context of causal prediction, we open new avenues of personalized support tailored to PPD and FMR1 carriers of different age groups.

Besides the frequency-time relations highlighted in the above exploration, the work also revealed important spatio-temporal features of the MMS. Namely, through examination of the joint empirical distributions of MMS derived from fluctuations in the angular speed peaks' amplitude and the MMS derived from the fluctuations in inter-peaks-interval timings, we found interdependences and complex patterns rendering invalid the common assumption of independence in the spikes data. This result also opens new questions about common assumptions of stationarity and homogeneity in the data. Future empirical and theoretical work will be necessary to advance this important area of research vital for interpretation and statistical inference of behavioral phenomena.

In summary, we offer a new unifying framework to stratify a random draw of the population based on natural walking patterns, identify subtypes withing each group and anticipate pathologies of the nervous systems bound to appear with natural aging and with genetic-based differences. Furthermore, we provide actionable models of noise cancellation to build supportive interventions with the potential to enhance causal prediction and feedback from movements and to improve internal temporal lags of information flow. This could help lower the cognitive load that an otherwise automatic walking task may cause as we naturally age, as we acquire Parkinsonism, or in cases where the person inherits a genetic mutation. Our personalized approach and our new definition of internal motor-sensing timings can provide true targeted interventions to help mitigate and protect against neurodegeneration.

Materials and Methods

This study was approved by the Rutgers Institutional Review Board (IRB) abiding by the precepts of the Helsinki Act. Thirty-seven patients were included out of thirty-eight participants (age mean 37.24, std 21.39, 10 males and 28 females). There was sensor malfunctioning for one elderly participant, so we did not include him in the analysis. Patients were recruited through the clinical_trials.gov site, the Robert Wood Johnson clinic, and the New Jersey Autism Center of Excellence (https://www.njace.us/). Informed consent was obtained from the participants according to our Rutgers University IRB-approved protocol. Different aspects of these data unrelated to gait, were previously published [8,9,66].

2.1. Experimental Design and Statistical Analyses

Participants wore the XSens system (17 wearable sensors across the body collecting position, orientation, and acceleration at 60Hz, from 23 joints depicted in Figure 11A). In-house MATLAB routines were used to implement the Frenet-Serret frame [67] and derive various kinematics parameters. Position was used to derive linear velocity fields, which were converted to scalar fields of speed (m/s). Then maxima and minima were obtained as landmarks to track the speed of the center of mass (e.g., Figure 11B) (obtained by replacing mass with length in the original equation 1).

$$V_{com} = \frac{\sum_{i=1}^{23} \mathrm{V}_i L_i}{\sum_{i=1}^{23} L_i} \quad (1)$$

Time series of the latter were scaled, and the micro-movement spikes (MMS) obtained in further analyses (Figure 11C).

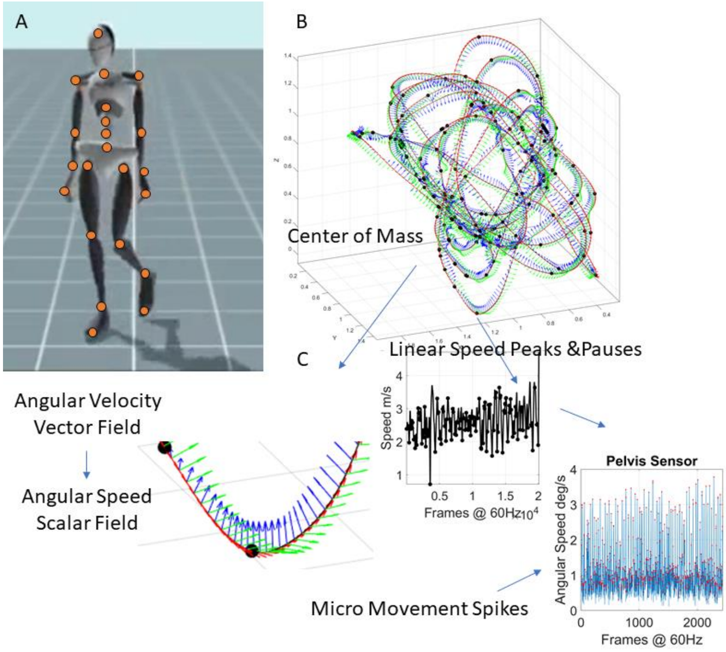

Figure 11: Methods Figure. (A) Data acquisition using a grid of wearable sensors calibrating position and orientation in real time and sampling changes of position in time, at 60Hz. (B) Center of Mass trajectories (m) in 3D parameterized using the Frenet-Serret frame to study geometric aspects of the curve. (C) Linear speed used to mark pauses and peaks along the curve, thus allowing us to express behavioral landmarks along other kinematics parameters such as the angular speed quantifying bodily rates of 23 joints' rotations. The MMS are derived from the fluctuations in angular speed amplitude. Red dots mark peaks (transitions of speed slope from positive to negative.)

Micromovement Spikes (MMS): The MMS are defined as the normalized peaks of any kinematics time series of the fluctuations in amplitude, as the signal deviates from the mean amplitude. Specifically, to obtain the micromovements time series from the angular speed time series we first calculate the peaks. Each peak is then normalized by the local average speed of the speed, *i.e.* the average value of the two minima before and after the peak (equation 2).

$$Npeak = \frac{peakV}{peakV + avgV_{localmin-to-localmin}} \quad (2)$$

It has been shown that the resulting MMS time series follows the generalized gamma distribution in human motion and applied to gait [33,68]. Then, from the resulting time series we subtract the gamma fitted mean (fitted using maximum likelihood estimation, MLE). The MMS time series allows us to extract information independent of the body dimensions of the subject. When tracking them continuously, we can used them as a peripheral proxy of the efferent an afferent activity of the central nervous system. Figure 12 shows the pipeline describing the MMS extraction from the sensor data.

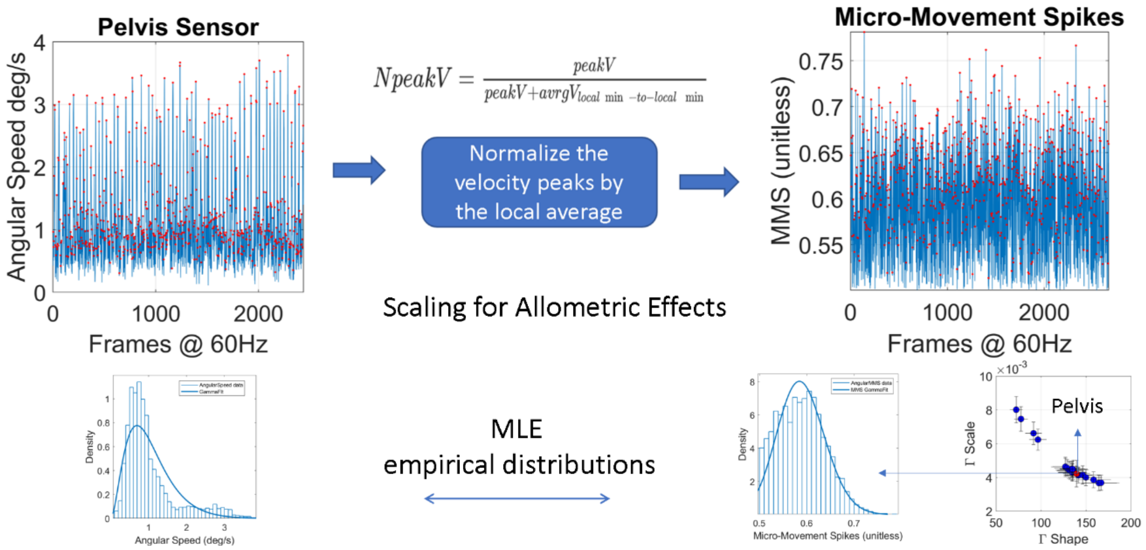

Figure 12: The MMS time series extraction from the angular speed tracking stochastic trajectories from all joints (red dot marks the pelvis for instance.)

Cross-coherence: The cross-coherence between two times series (assumed to be the realizations of unknown stochastic processes) is defined as the cross-spectral density between the two series normalized by the product of their auto-spectral densities [69]. Since human motion is non-linear, in this study we use cross-coherence to quantify the similarity between any two body nodes' MMS time series in the frequency domain. We then identify the frequency for which the cross-coherence function is maximized.

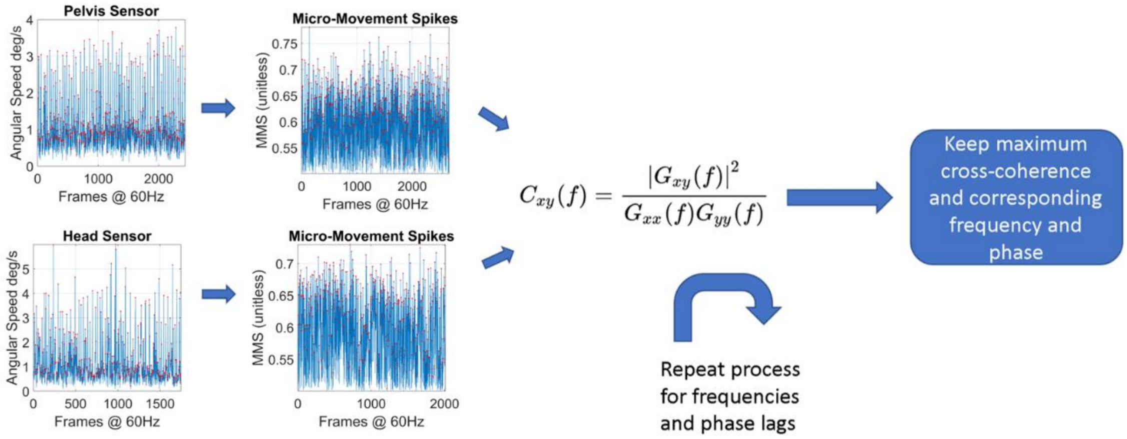
Pelvis Sensor
Angular Speed deg/s
Frames @ 60Hz
Micro-Movement Spikes
MMS (unitless)
Frames @ 60Hz
Head Sensor
Angular Speed deg/s
Frames @ 60Hz
Micro-Movement Spikes
MMS (unitless)
Frames @ 60Hz
$C_{xy}(f) = \frac{|G_{xy}(f)|^2}{G_{xx}(f)G_{yy}(f)}$
Keep maximum cross-coherence and corresponding frequency and phase
Repeat process for frequencies and phase lags

Figure 13: The pipeline for the calculation of the maximum cross-coherence and the frequency for which it is maximized.

Mean frequency: The mean frequency of a spectrogram $P(f)$ is calculated as:

$$f_{mean} = \frac{\sum_{j=1}^{N} f_j P_j}{\sum_{j=1}^{N} P_j} \quad (3)$$

Where f_j is the central frequency of the j-th bin of the spectrum and P_j the corresponding value of the power spectral density. N is the total number of bins [70].

Granger causality: The MMS serve as a proxy to reflect the inner activity of the nervous system as it is expressed by the kinematics of the various body parts. Hence, we now have a network of times series (23 nodes) that provide information about the mechanisms of the CNS to control the peripheral activity for each subject and each group of subjects. Specifically, we are interested in the relationship between two time series of MMS. Traditional concepts, such as mutual information, cross-correlation and cross-coherence are being widely used to estimate the mutual information between two stochastic processes [71], or to investigate how one relates to the other in the time or frequency domain [9,72,73]. However, they provide no information about the direction in which the information flows, i.e., which stochastic process is the cause and which the effect.

Other concepts such as Transfer Entropy (TE) and Granger Causality (GC) give us both the direction in which the information flows, as well as the quantity of the information flowing from the causal stochastic process to the effector stochastic process [74]. In fact, in the case of gaussian processes these two are equivalent [75]. TE does not require a model and is based on information theory concepts. GC on the other hand, requires fitting an AR model of order N to the time series data.

For the purposes of this paper, we choose the concept of GC. There are two reasons for our choice. First, GC has a much smaller computational complexity than TE. Second, assuming an autoregressive model can help us estimate the response lags between different body activities. We define the response lag as the number of MM peaks needed for information to flow from the afferent input of a body part to the efferent output of another body part. To explain how we estimate the response lags between the activities of any two body parts we must first explain the concept of GC.

Granger, in his original paper defined causality for a pair of stochastic processes X and Y in a solid, mathematical way [45]. Assume we have a closed system or "universe" in which all available information is contained in the stochastic processes X and Y and let X_t and Y_t be the realizations of these stochastic processes up to time t. Let U_t be all the information accumulated from both time series up to *t-1*. U-Y implies all information apart from Y. Granger gave the following definition of causality. Using his own words [45]:

"If $\sigma^2(X|U)$<$\sigma^2(X|U-Y)$, we say that Y is causing X, denoted by Y_t => X_t. We say that Y_t is causing X_t, if we are better able to predict X_t using all available information than if the information apart from Y_t has been used."

The operator $A|B$, where A, B are stochastic processes means the "construction" of a model where A is predicted from B. The operator $\sigma^2(A|B)$ means the variance of the error of the model $A|B$. Granger's definition implies that if a model that predicts the dynamic behavior of X that does not include Y, has a greater on average error than a model that includes Y, then Y "causes" X in that sense. Furthermore, Granger gave a formal definition of "causality lag", which simply informs us how far in the past we should consider samples of X and Y in our prediction to get an optimal prediction.

"If Y_t => X_t, we define the (integer) causality lag m to be the least value of k such that $\sigma^2(X|U-Y(k))$<$\sigma^2(X|U-Y(k+1))$. Thus, knowing the values Y_{t-j}, *j=0,1,…m-1*, will be of no help in improving the prediction of X_t."

Simply put, the concept of causality lag refers to the maximum lag in the past of the realization of the stochastic process Y, beyond which, including more past samples will result in a bigger prediction error.

Granger also referred to "instantaneous causality", which simply means that in the prediction we also include the present values of the stochastic processes. In our present work, due to the non-instantaneous nature of neural information, we assume that prediction should include only the past values. In his solution to the problem of estimating causality for econometric time series, Granger assumed autoregressive models of some appropriate order and used techniques of spectral analysis [64]. He defined two models, one simple causal model that includes the past samples of both time series and one non-causal model that includes only the effector process. For our purposes, we formulated our own model and approach to Granger causality which allows us to quantify the internal motor timings of the system.

Let X and Y be the two univariate stochastic processes and X_n, Y_n the corresponding time series we obtained from our sensors. For a choice l of the internal time lag of the system, we assume the non-causal and causal models:

$$x_n = a_1 x_{n-l} + w_{1n} \quad (4)$$

$$x_n = a_2 x_{n-l} + b y_{n-l} + w_{2n} \quad (5)$$

Where w_1, w_2 are independent discrete time AWGN (additive white gaussian noise) processes and a_1, a_2, b constants we want to estimate from the statistical properties of our data. We also make the hypothesis that the noise processes are independent from X and Y. Assuming that the noise processes are gaussian implies they have zero means. To apply this model without loss of generality we simply pre-process our data by centering them around zero.

To proceed, we multiply equation (4) with x_n and we get:

$$x_n^2 = a x_n x_{n-l} + w_{1n} x_n \quad (6)$$

Applying the expectation operator $E(.)$ on both sides of equation (6):

$$E\{x_n^2\} = aE\{x_n x_{n-l}\} + E\{w_{1n} x_n\} \quad (7)$$

Since noise w_1 and the process X are independent, it means they are uncorrelated. Therefore:

$$E\{x_n^2\} = aE\{x_n x_{n-l}\}$$

From which we get an estimate for the constant a:

$$a = \frac{E\{x_n^2\}}{E\{x_n x_{n-l}\}} = \frac{R_{xx}(0)}{Rxx(l)} \quad (8)$$

Where $R_{xx}(\tau) = E\{x_n x_{n-\tau}\}$ is the autocorrelation function of X.

We continue by multiplying (5) with x_n:

$$x_n^2 = a_2 x_{n-l} x_n + b y_{n-l} x_n + w_{2n} x_n \quad (9)$$

Also, we multiply (5) with x_{n-l} :

$$x_n x_{n-l} = a_2 x_{n-l}^2 + b y_{n-l}\, x_{n-l} + w_{2n} x_{n-l} \quad (10)$$

Taking the expectation on both sides of (9) and (10), since X and Y are uncorrelated, we finally arrive to the system of equations:

$$R_{xx}(0) = a_2 R_{xx}(l) + b R_{xy}(l)$$

$$R_{xx}(l) = a_2 R_{xx}(0) + b R_{xy}(0) \qquad (11)$$

Where $R_{xy}(\tau) = E\{x_n y_{n-\tau}\}$ is the cross-correlation function between X and Y.

Assuming (11) has a solution, we can estimate a_2, b .

The final step in our analysis is to find the variances of the noises.

We square equations (4) and (5):

$$x_n^2 = a_1^2 x_{n-l}^2 + w_{1n}^2 + 2a_1 x_{n-l} w_{1n} \quad (12)$$

$$x_n^2 = a_2^2 x_{n-l}^2 + b^2 y_{n-l}^2 + w_{2n}^2 + 2a_2 x_{n-l} b y_{n-l} + 2(a_2 x_{n-l} w_{2n} + b y_{n-l} w_{2n}) \quad (13)$$

Applying the expectation in both sides, since the noises are independent of the processes, all cross- correlation terms between processes and noises are zero, therefore:

$$E\{w_{1n}^2\} = E\{x_n^2\} - a_1^2 E\{x_{n-l}^2\} \quad (14)$$

$$E\{w_{2n}^2\} = E\{x_n^2\} - a_2^2 E\{x_{n-l}^2\} - b^2 E\{y_{n-l}^2\} - 2a_2 b E\{x_{n-l} y_{n-l}\} \quad (15)$$

Since the variance of a noise processes w is $\sigma^2 = E\{(w - w_{mean})^2\}$, in our case where the noises are zero mean, eventually:

$$\sigma_1^2 = R_{xx}(0) - a_1^2 R_{xx}(0) = (1 - a_1^2) R_{xx}(0) \quad \mathit{(16)}$$

$$\sigma_2^2 = R_{xx}(0) - a_2^2 R_{xx}(0) - b^2 R_{yy}(0) - 2a_2 b R_{xy}(0) = (1 - a_2^2) R_{xx}(0) - 2a_2 b R_{xy}(0) \quad \mathit{(17)}$$

Thus, solving system (9) gives us the constants of the system for a given choice of lag and then equations (16), (17) give us the errors of the non-causal and causal models. Following the logarithmic definition of causality[76]:

$$GC = \log\left(\frac{\sigma_1^2}{\sigma_2^2}\right) \quad (18)$$

If the causal model better predicts the behavior of X for a given internal motor lag, $\sigma_2^2 < \sigma_1^2$ then $GC > 0$.

A standard causal autoregressive (AR) model of order one is of the form:

$$x_n = ax_{n-1} + by_{n-1} + noise$$

Which is order 1. However, what is the physical meaning of "order 1"? It means we assume the previous sample, one lag in the past of X, contribute to the prediction of X. It is an arbitrary quantity when we consider it independently of the sampling rate F_s of our sensors. In context however, one lag is $\frac{1}{F_s}$ seconds, which is the fundamental unit of time of our system. In our model, we assume:

$$x_n = ax_{n-l} + by_{n-l} + noise$$

This can still be assumed an autoregressive model of order 1 in which the fundamental unit of time is not one sampling period but l sampling periods. Different choices of l will give autoregressive models for different ***time scales.*** The time scale l for which causality is maximized is our definition of "internal motor timing", because at this time scale, we have the maximum flow of information from Y to X.

We make the following hypothesis. At any given moment, the process Y_t transmits information to the process X_t through the CNS. The response lag between the two processes is the time needed for information to travel from the afferent process Y_t to the efferent process X_t. Following this train of thought we can assume that the lag parameter of the AR models that maximizes the GC is the best estimation of the corresponding response time between X_t and Y_t. Therefore, we propose the following pipeline of analysis to find the maximum GC and estimate the response lags between any two sensor MMS time series of the subjects (Figure 14).

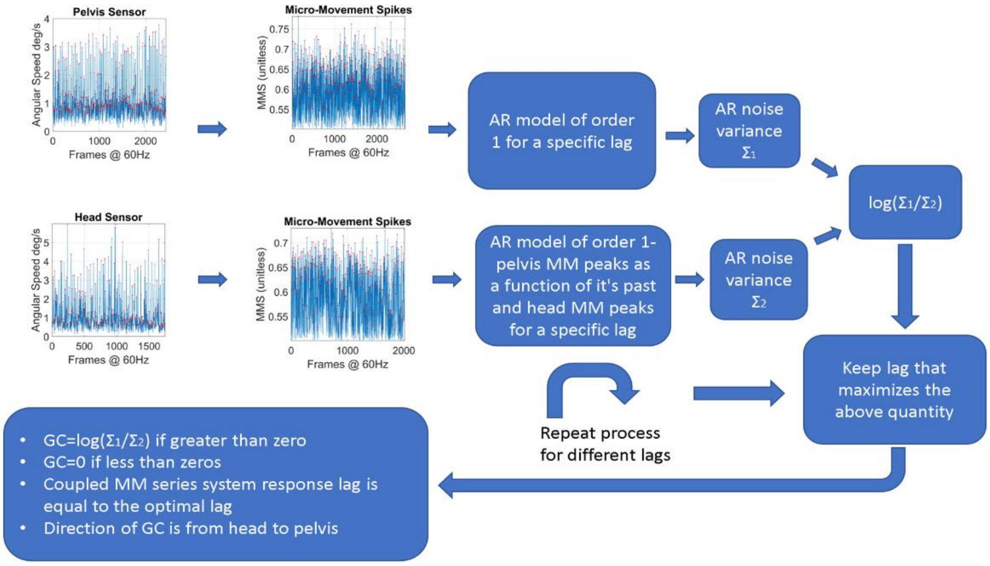
Pelvis Sensor
Angular Speed deg/s
Frames @ 60Hz
Micro-Movement Spikes
MMS (unitless)
Frames @ 60Hz
AR model of order 1 for a specific lag
AR noise variance Σ1
log(Σ1/Σ2)
Head Sensor
Angular Speed deg/s
Frames @ 60Hz
Micro-Movement Spikes
MMS (unitless)
Frames @ 60Hz
AR model of order 1- pelvis MM peaks as a function of it's past and head MM peaks for a specific lag
AR noise variance Σ2
Keep lag that maximizes the above quantity
Repeat process for different lags
GC=log(Σ1/Σ2) if greater than zero
GC=0 if less than zeros
Coupled MM series system response lag is equal to the optimal lag
Direction of GC is from head to pelvis

Figure 14: Pipeline for the estimation of the Granger Causality and Response time values between two body parts.

References

1 Ambar Akkaoui, M., Geoffroy, P. A., Roze, E., Degos, B. & Garcin, B. Functional Motor Symptoms in Parkinson's Disease and Functional Parkinsonism: A Systematic Review. *J Neuropsychiatry Clin Neurosci* **32**, 4-13, doi:10.1176/appi.neuropsych.19030058 (2020).

2 Chien, J. H., Yentes, J., Stergiou, N. & Siu, K. C. The Effect of Walking Speed on Gait Variability in Healthy Young, Middle-aged and Elderly Individuals. *J Phys Act Nutr Rehabil* **2015** (2015).

3 Doridam, J., Mongin, M. & Degos, B. Movement disorders in the elderly. *Geriatr Psychol Neuropsychiatr Vieil* **17**, 395-404, doi:10.1684/pnv.2019.0825 (2019).

4 Lenardt, M. H. *et al.* Gait speed and cognitive score in elderly users of the primary care service. *Rev Bras Enferm* **68**, 1163-1168, doi:10.1590/0034-7167.2015680623i (2015).

5 Parisi, F. *et al.* Body-Sensor-Network-Based Kinematic Characterization and Comparative Outlook of UPDRS Scoring in Leg Agility, Sit-to-Stand, and Gait Tasks in Parkinson's Disease. *IEEE J Biomed Health Inform* **19**, 1777-1793, doi:10.1109/JBHI.2015.2472640 (2015).

6 Park, S. H. *et al.* Functional motor control deficits in older FMR1 premutation carriers. *Exp Brain Res* **237**, 2269-2278, doi:10.1007/s00221-019-05566-3 (2019).

7 Wang, Z., Khemani, P., Schmitt, L. M., Lui, S. & Mosconi, M. W. Static and dynamic postural control deficits in aging fragile X mental retardation 1 (FMR1) gene premutation carriers. *J Neurodev Disord* **11**, 2, doi:10.1186/s11689-018-9261-x (2019).

8 Ryu, J., Vero, J., Dobkin, R. D. & Torres, E. B. Dynamic Digital Biomarkers of Motor and Cognitive Function in Parkinson's Disease. *J Vis Exp*, doi:10.3791/59827 (2019).

9 Ryu, J., Vero, J. & Torres, E. B. in *MOCO '17: Proceedings of the 4th International Conference on Movement Computing.* 1-8 (ACM).

10 Torres, E. B. *et al.* Characterization of the Statistical Signatures of Micro-Movements Underlying Natural Gait Patterns in Children with Phelan McDermid Syndrome: Towards Precision-Phenotyping of Behavior in ASD. *Front Integr Neurosci* **10**, 22, doi:10.3389/fnint.2016.00022 (2016).

11 Torres, E. B. Reframing Psychiatry for Precision Medicine. *J Pers Med* **10**, doi:10.3390/jpm10040144 (2020).

12 Fujita-Jimbo, E. *et al.* Mutation in Parkinson disease-associated, G-protein-coupled receptor 37 (GPR37/PaelR) is related to autism spectrum disorder. *PLoS One* **7**, e51155, doi:10.1371/journal.pone.0051155 (2012).

13 Glessner, J. T. *et al.* Autism genome-wide copy number variation reveals ubiquitin and neuronal genes. *Nature* **459**, 569-573, doi:10.1038/nature07953 (2009).

14 Xie, F. *et al.* Advances in the Research of Risk Factors and Prodromal Biomarkers of Parkinson's Disease. *ACS Chem Neurosci* **10**, 973-990, doi:10.1021/acschemneuro.8b00520 (2019).

15 Amadori, K. & Steiner, T. [Parkinson's syndromes in geriatric patients : Epidemiological, clinical and therapeutic characteristics]. *Nervenarzt* **90**, 1279-1291, doi:10.1007/s00115-019-00825-8 (2019).

16 Lord, C. *et al.* Autism diagnostic observation schedule: a standardized observation of communicative and social behavior. *J Autism Dev Disord* **19**, 185-212 (1989).

17 (American Psychiatric Association, Arlington, VA, 2013).

18 Hagerman, R., Hoem, G. & Hagerman, P. Fragile X and autism: Intertwined at the molecular level leading to targeted treatments. *Mol Autism* **1**, 12, doi:10.1186/2040-2392-1-12 (2010).

19 Hall, D. A. *et al.* Clinimetric Properties of the Fragile X-associated Tremor Ataxia Syndrome Rating Scale. *Mov Disord Clin Pract* **6**, 120-124, doi:10.1002/mdc3.12708 (2019).

20 Leehey, M. A. *et al.* FMR1 CGG repeat length predicts motor dysfunction in premutation carriers. *Neurology* **70**, 1397-1402, doi:10.1212/01.wnl.0000281692.98200.f5 (2008).

21 Torres, E. B., Caballero, C. & Mistry, S. Aging with Autism Departs Greatly from Typical Aging. *Sensors (Basel)* **20**, doi:10.3390/s20020572 (2020).

22 Torres, E. B. & Denisova, K. Motor noise is rich signal in autism research and pharmacological treatments. *Sci Rep* **6**, 37422, doi:10.1038/srep37422 (2016).

23 de Rijk, M. C. *et al.* Prevalence of parkinsonism and Parkinson's disease in Europe: the EUROPARKINSON Collaborative Study. European Community Concerted Action on the Epidemiology of Parkinson's disease. *J Neurol Neurosurg Psychiatry* **62**, 10-15, doi:10.1136/jnnp.62.1.10 (1997).

24 Starkstein, S., Gellar, S., Parlier, M., Payne, L. & Piven, J. High rates of parkinsonism in adults with autism. *J Neurodev Disord* **7**, 29, doi:10.1186/s11689-015-9125-6 (2015).

25 Caballero, C., Mistry, S. & Torres, E. B. Age-Dependent Statistical Changes of Involuntary Head Motion Signatures Across Autism and Controls of the ABIDE Repository. *Front. Integr. Neurosci.* **14**, 1-14, doi:doi: 10.3389/fnint.2020.00023 (2020).

26 Hall, D. A., Howard, K., Hagerman, R. & Leehey, M. A. Parkinsonism in FMR1 premutation carriers may be indistinguishable from Parkinson disease. *Parkinsonism Relat Disord* **15**, 156-159, doi:10.1016/j.parkreldis.2008.04.037 (2009).

27 Wang, L. W., Berry-Kravis, E. & Hagerman, R. J. Fragile X: leading the way for targeted treatments in autism. *Neurotherapeutics* **7**, 264-274, doi:10.1016/j.nurt.2010.05.005 (2010).

28 Godoi, B. B. *et al.* Parkinson's disease and wearable devices, new perspectives for a public health issue: an integrative literature review. *Rev Assoc Med Bras (1992)* **65**, 1413-1420, doi:10.1590/1806-9282.65.11.1413 (2019).

29 O'Keeffe, C. *et al.* Complexity based measures of postural stability provide novel evidence of functional decline in fragile X premutation carriers. *J Neuroeng Rehabil* **16**, 87, doi:10.1186/s12984-019-0560-6 (2019).

30 Schmitt, A. C., Daniels, J. N., Baudendistel, S. T., Okun, M. S. & Hass, C. J. The Primary Gait Screen in Parkinson's disease: Comparison to standardized measures. *Gait Posture* **73**, 71-73, doi:10.1016/j.gaitpost.2019.07.132 (2019).

31 Torres, E. B. *et al.* Toward Precision Psychiatry: Statistical Platform for the Personalized Characterization of Natural Behaviors. *Front Neurol* **7**, 8, doi:10.3389/fneur.2016.00008 (2016).

32 Granger, C. W. J. *Spectral analysis of economic time series*. (Princeton University Press, 1964).

33 Torres, E. B. *et al.* Autism: the micro-movement perspective. *Front Integr Neurosci* **7**, 32, doi:10.3389/fnint.2013.00032 (2013).

34 Von Holst E. & H., M. in *Perceptual Processing: Stimulus equivalence and pattern recognition* (ed ed Dodwell PC) 41-72 (Appleton-Century-Crofts, 1950).

35 Torres, E. B. Two classes of movements in motor control. *Exp Brain Res* **215**, 269-283, doi:10.1007/s00221-011-2892-8 (2011).

36 Wolpert, D. M., Miall, R. C. & Kawato, M. Internal models in the cerebellum. *Trends Cogn Sci* **2**, 338-347, doi:10.1016/s1364-6613(98)01221-2 (1998).

37 Kawato, M. & Wolpert, D. Internal models for motor control. *Novartis Found Symp* **218**, 291-304; discussion 304-297, doi:10.1002/9780470515563.ch16 (1998).

38 Ryu, J. & Torres, E. The Autonomic Nervous System Differentiates between Levels of Motor Intent and End Effector. *J Pers Med* **10**, doi:10.3390/jpm10030076 (2020).

39 Torres, E. B. System and method for determining amount of volition in a subject. US patent (2017, Oct. 19).

40 Torres, E. B. Signatures of movement variability anticipate hand speed according to levels of intent. *Behav Brain Funct* **9**, 10, doi:10.1186/1744-9081-9-10 (2013).

41 Anderson, S. R. *et al.* Adaptive cancelation of self-generated sensory signals in a whisking robot. *IEEE Transactions on Robotics* **26**, 1065-1076 (2010).

42 Anderson, S. R. *et al.* An internal model architecture for novelty detection: implications for cerebellar and collicular roles in sensory processing. *PLoS One* **7**, e44560 (2012).

43 Bays, P. M. & Wolpert, D. M. Computational principles of sensorimotor control that minimize uncertainty and variability. *The Journal of physiology* **578**, 387-396 (2007).

44 Habra, T., Grotz, M., Sippel, D., Asfour, T. & Ronsse, R. in *2017 IEEE-RAS 17th International Conference on Humanoid Robotics (Humanoids).* 47-54 (IEEE).

45 Granger, C. W. J. Investigating Causal Relations by Econometric Models and Cross-spectral Methods. *Econometrica* **37**, 424-438 (1969).

46 Hartigan, J. A. & Hartigan, P. M. The Dip Test of Unimodality. *The Annals of Statistics* **13**, 70-84 (1985).

47 Lee, H. J. *et al.* Tremor frequency characteristics in Parkinson's disease under resting-state and stress-state conditions. *Journal of the neurological sciences* **362**, 272-277 (2016).

48 Viviani, P. & Flash, T. Minimum-jerk, two-thirds power law, and isochrony: converging approaches to movement planning. *Journal of Experimental Psychology: Human Perception and Performance* **21**, 32 (1995).

49 Kawato, M., Maeda, Y., Uno, Y. & Suzuki, R. Trajectory formation of arm movement by cascade neural network model based on minimum torque-change criterion. *Biological cybernetics* **62**, 275-288 (1990).

50 Alexander, R. M. A minimum energy cost hypothesis for human arm trajectories. *Biological cybernetics* **76**, 97-105 (1997).

51 Doya, K. Complementary roles of basal ganglia and cerebellum in learning and motor control. *Current opinion in neurobiology* **10**, 732-739 (2000).

52 Peters, J. & Schaal, S. Reinforcement learning of motor skills with policy gradients. *Neural networks* **21**, 682-697 (2008).

53 Buhusi, C. V. & Meck, W. H. What makes us tick? Functional and neural mechanisms of interval timing. *Nature reviews neuroscience* **6**, 755-765 (2005).

54 Lestienne, R. Spike timing, synchronization and information processing on the sensory side of the central nervous system. *Progress in neurobiology* **65**, 545-591 (2001).

55 Machado, A., Malheiro, M. T. & Erlhagen, W. Learning to time: A perspective. *Journal of the experimental analysis of behavior* **92**, 423-458 (2009).

56 Simen, P., Rivest, F., Ludvig, E. A., Balci, F. & Killeen, P. Timescale invariance in the pacemaker-accumulator family of timing models. *Timing & Time Perception* **1**, 159-188 (2013).

57 Flash, T., Hogan, N. The coordination of arm movements: an experimentally confirmed mathematical model. *The Journal of Neuroscience* **5**, 1688-1703 (1985).

58 Torres, E. B., Quian Quiroga, R., Cui, H. & Buneo, C. A. Neural correlates of learning and trajectory planning in the posterior parietal cortex. *Front Integr Neurosci* **7**, 39, doi:10.3389/fnint.2013.00039 (2013).

59 Torres, E. B., Zipser, D. Reaching to Grasp with a Multi-jointed Arm (I): A Computational Model. *Journal of Neurophysiology* **88**, 1-13 (2002).

60 Torres, E. & Andersen, R. Space-time separation during obstacle-avoidance learning in monkeys. *J Neurophysiol* **96**, 2613-2632, doi:10.1152/jn.00188.2006 (2006).

61 Torres, E. B., Heilman, K. M. & Poizner, H. Impaired endogenously evoked automated reaching in Parkinson's disease. *J Neurosci* **31**, 17848-17863, doi:10.1523/JNEUROSCI.1150-11.2011 (2011).

62 Yin, H. H. Action, time and the basal ganglia. *Philos Trans R Soc Lond B Biol Sci* **369**, 20120473, doi:10.1098/rstb.2012.0473 (2014).

63 Yin, H. H. The Basal Ganglia in Action. *Neuroscientist* **23**, 299-313, doi:10.1177/1073858416654115 (2017).

64 Granger, C. W. Investigating causal relations by econometric models and cross-spectral methods. *Econometrica: journal of the Econometric Society*, 424-438 (1969).

65 Gallistel, C. R. & Gibbon, J. Time, rate, and conditioning. *Psychol Rev* **107**, 289-344, doi:10.1037/0033-295x.107.2.289 (2000).

66 Bokadia, H., Rai, R. & Torres, E. B. Digitized ADOS: Social Interactions beyond the Limits of the Naked Eye. *J Pers Med* **10**, doi:10.3390/jpm10040159 (2020).

67 Do Carmo, M. *Differential Geometry of Curves and Surfaces*. (Prentice Hall, 1976).

68 Torres, E. B. *Objective biometric methods for the diagnosis and treatment of nervous system disorders*. (Academic Press, 2018).

69 Ghaderi, A. H. *et al.* Time estimation and beta segregation: An EEG study and graph theoretical approach. *PLoS One* **13**, e0195380 (2018).

70 Phinyomark, A., Thongpanja, S., Hu, H., Phukpattaranont, P. & Limsakul, C. The usefulness of mean and median frequencies in electromyography analysis. *Computational intelligence in electromyography analysis-A perspective on current applications and future challenges*, 195-220 (2012).

71 Wang, T., Bebbington, M. S. & Harte, D. S. A comparative study of coherence, mutual information and cross-intensity models. *International Journal of Information and Systems Sciences* **6**, 49-60 (2008).

72 Ryu, J. & Torres, E. B. Characterization of Sensory-Motor Behavior Under Cognitive Load Using a New Statistical Platform for Studies of Embodied Cognition. *Front. Hum. Neurosci.* **12**, 1-19, doi:10.3389/fnhum.2018.00116 (2018).

73 Kalampratsidou, V. & Torres, E. B. Peripheral Network Connectivity Analyses for the Real-Time Tracking of Coupled Bodies in Motion. *Sensors (Basel)* **18**, doi:10.3390/s18093117 (2018).

74 Vicente, R., Wibral, M., Lindner, M. & Pipa, G. Transfer entropy—a model-free measure of effective connectivity for the neurosciences. *Journal of computational neuroscience* **30**, 45-67 (2011).

75 Barnett, L., Barrett, A. B. & Seth, A. K. Granger causality and transfer entropy are equivalent for Gaussian variables. *Physical review letters* **103**, 238701 (2009).

76 Ding, M., Chen, Y. & Bressler, S. L. 17 Granger causality: basic theory and application to neuroscience. *Handbook of time series analysis: recent theoretical developments and applications* **437** (2006).

Author Contributions: T.B. and E.B.T. conceptualized the study, designed the methodology and wrote the software. T.B. did the validation, investigation, and formal analysis. T.B and E.B.T. designed the figures / visualization tools. R.R. and J.R. did the data collection and curation. T.B. and E.B.T. did the original writing—original draft preparation, and all authors reviewed and edited the MS to its final state. E.B.T. did the project supervision, administration, and funding acquisition. All authors have read and agreed to the published version of the manuscript.

Funding: This research was funded by The New Jersey Governor's Council for the Medical Research and Treatments of Autism, grant number CAUT15APL038 and by the Nancy Lurie Marks Family Foundation Career Development Award to EBT.

Acknowledgments: We thank all participants in the study.

Conflicts of Interest: The authors declare no conflict of interest. The funders had no role in the design of the study; in the collection, analyses, or interpretation of data; in the writing of the manuscript, or in the decision to publish the results.

© 2021 by the authors. Submitted for possible open access publication under the terms and conditions of the Creative Commons Attribution (CC BY) license (http://creativecommons.org/licenses/by/4.0/).

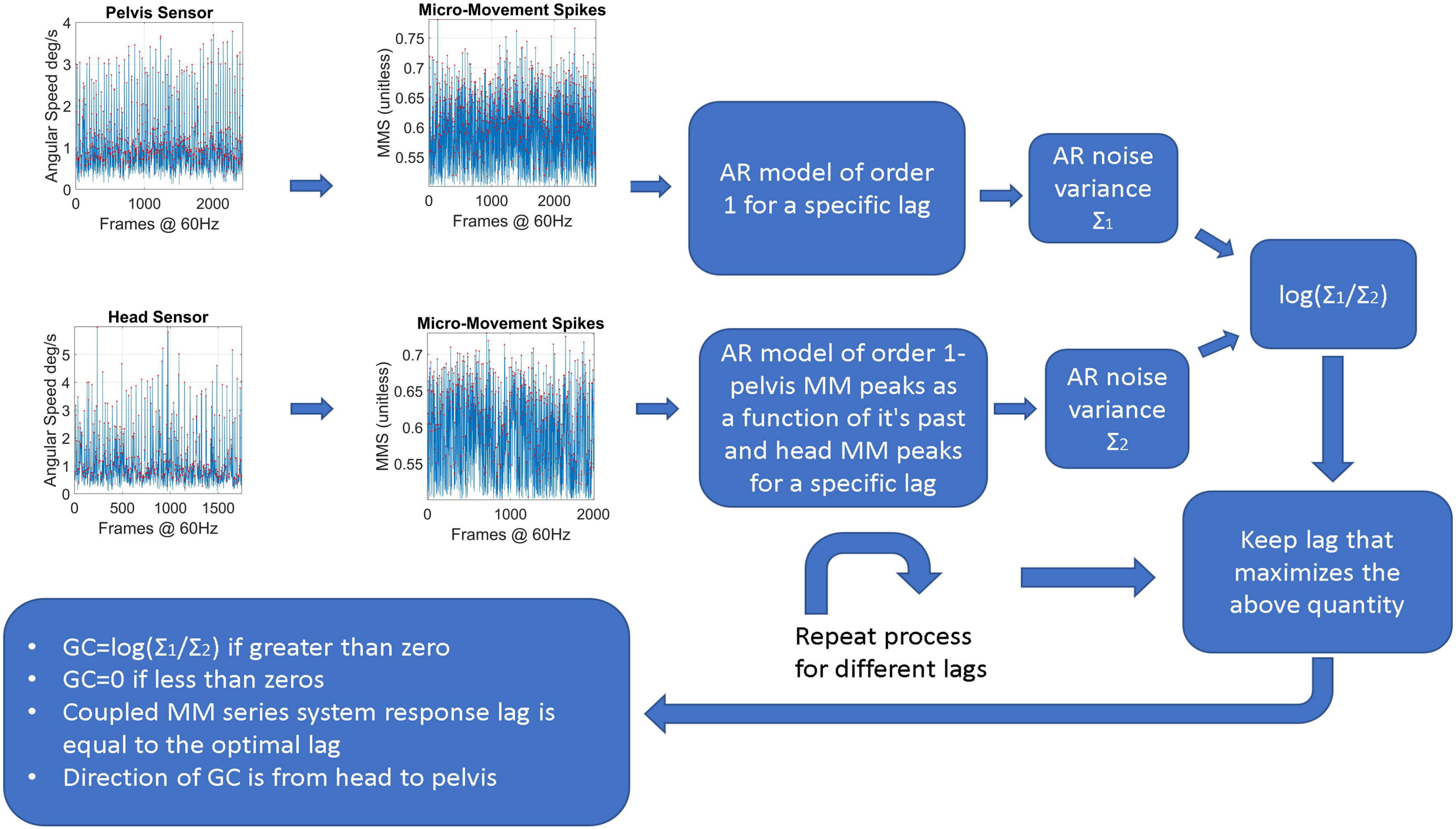
Pelvis Sensor
Angular Speed deg/s
0
1
2
3
4
0
1000
2000
Frames @ 60Hz
Micro-Movement Spikes
MMS (unitless)
0.55
0.6
0.65
0.7
0.75
0
1000
2000
Frames @ 60Hz
Head Sensor
Angular Speed deg/s
0
1
2
3
4
5
0
500
1000
1500
Frames @ 60Hz
Micro-Movement Spikes
MMS (unitless)
0.55
0.6
0.65
0.7
0
1000
2000
Frames @ 60Hz

AR model of order 1 for a specific lag

AR noise variance Σ_1

AR model of order 1- pelvis MM peaks as a function of it's past and head MM peaks for a specific lag

AR noise variance Σ_2

$\log(\Sigma_1/\Sigma_2)$

Keep lag that maximizes the above quantity

Repeat process for different lags

- GC=$\log(\Sigma_1/\Sigma_2)$ if greater than zero
- GC=0 if less than zeros
- Coupled MM series system response lag is equal to the optimal lag
- Direction of GC is from head to pelvis

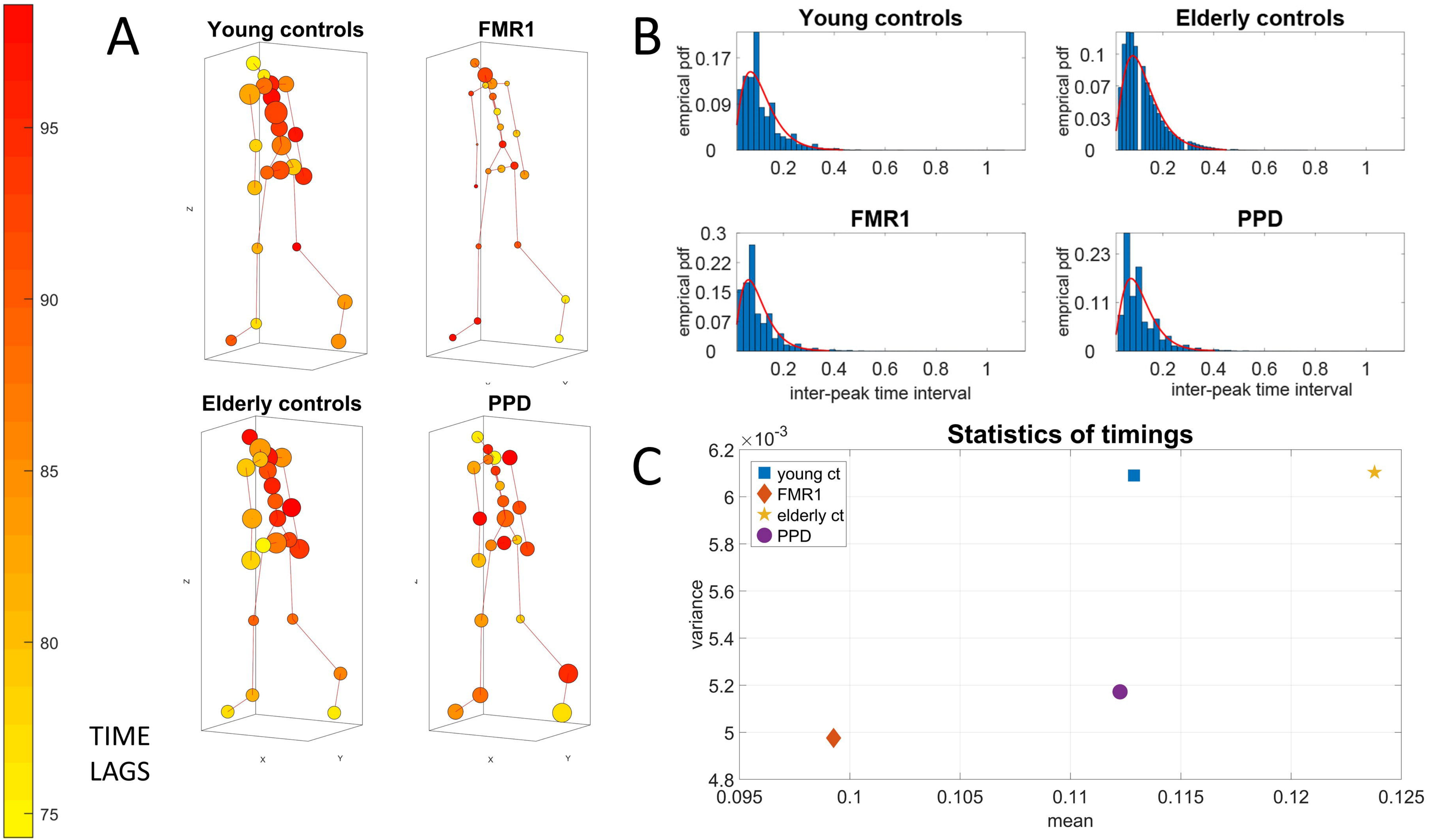
A
Young controls
FMR1
Elderly controls
PPD
TIME LAGS
95
90
85
80
75
z
x
y
B
Young controls
Elderly controls
FMR1
PPD
emprical pdf
inter-peak time interval
0.17
0.09
0
0.1
0.07
0.03
0.3
0.22
0.15
0.23
0.11
0.2
0.4
0.6
0.8
1
C
Statistics of timings
×10^-3
variance
mean
young ct
FMR1
elderly ct
PPD
6.2
6
5.8
5.6
5.4
5.2
5
4.8
0.095
0.1
0.105
0.11
0.115
0.12
0.125

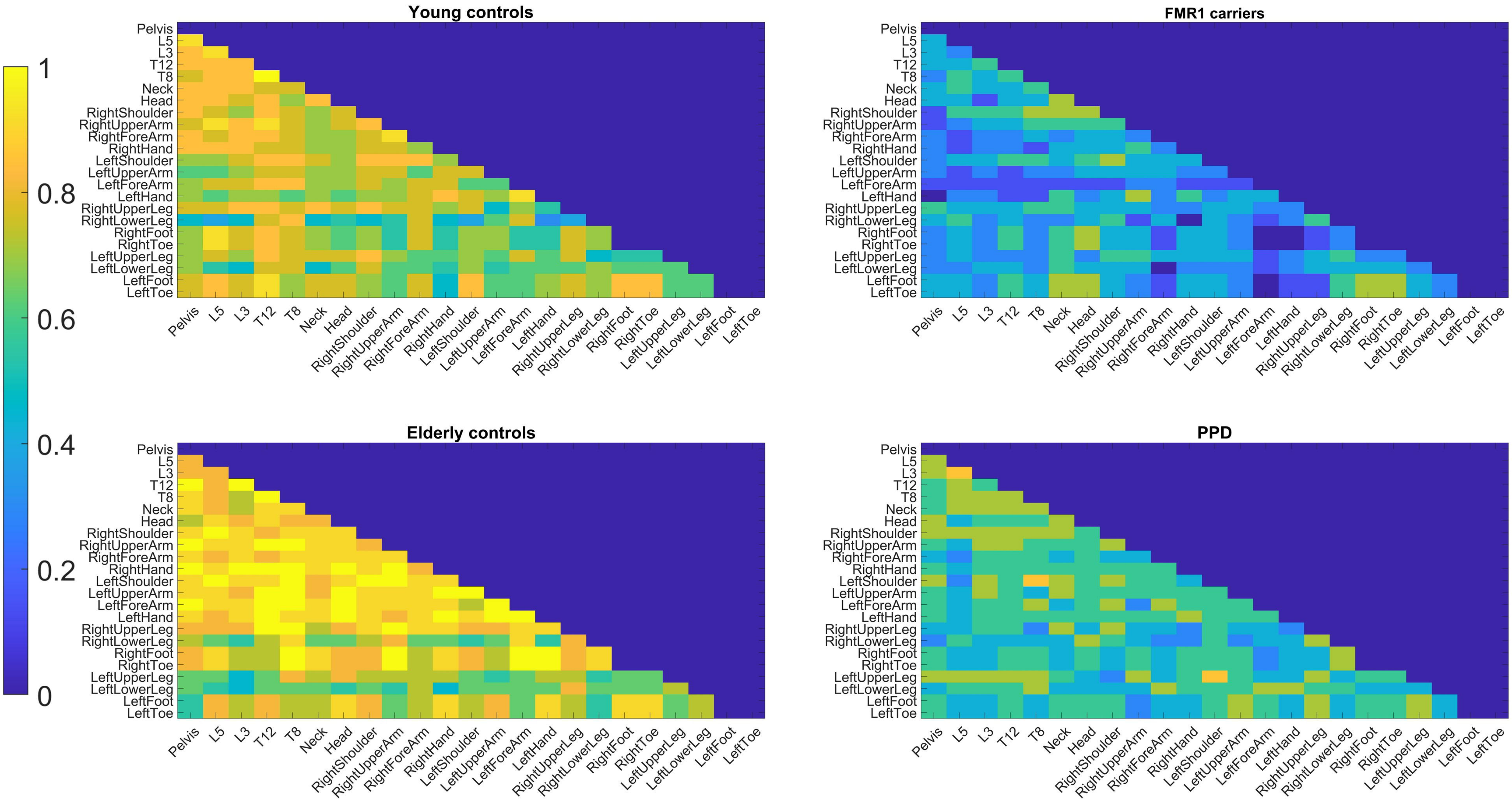
1
0.8
0.6
0.4
0.2
0
Young controls
FMR1 carriers
Elderly controls
PPD
Pelvis
L5
L3
T12
T8
Neck
Head
RightShoulder
RightUpperArm
RightForeArm
RightHand
LeftShoulder
LeftUpperArm
LeftForeArm
LeftHand
RightUpperLeg
RightLowerLeg
RightFoot
RightToe
LeftUpperLeg
LeftLowerLeg
LeftFoot
LeftToe

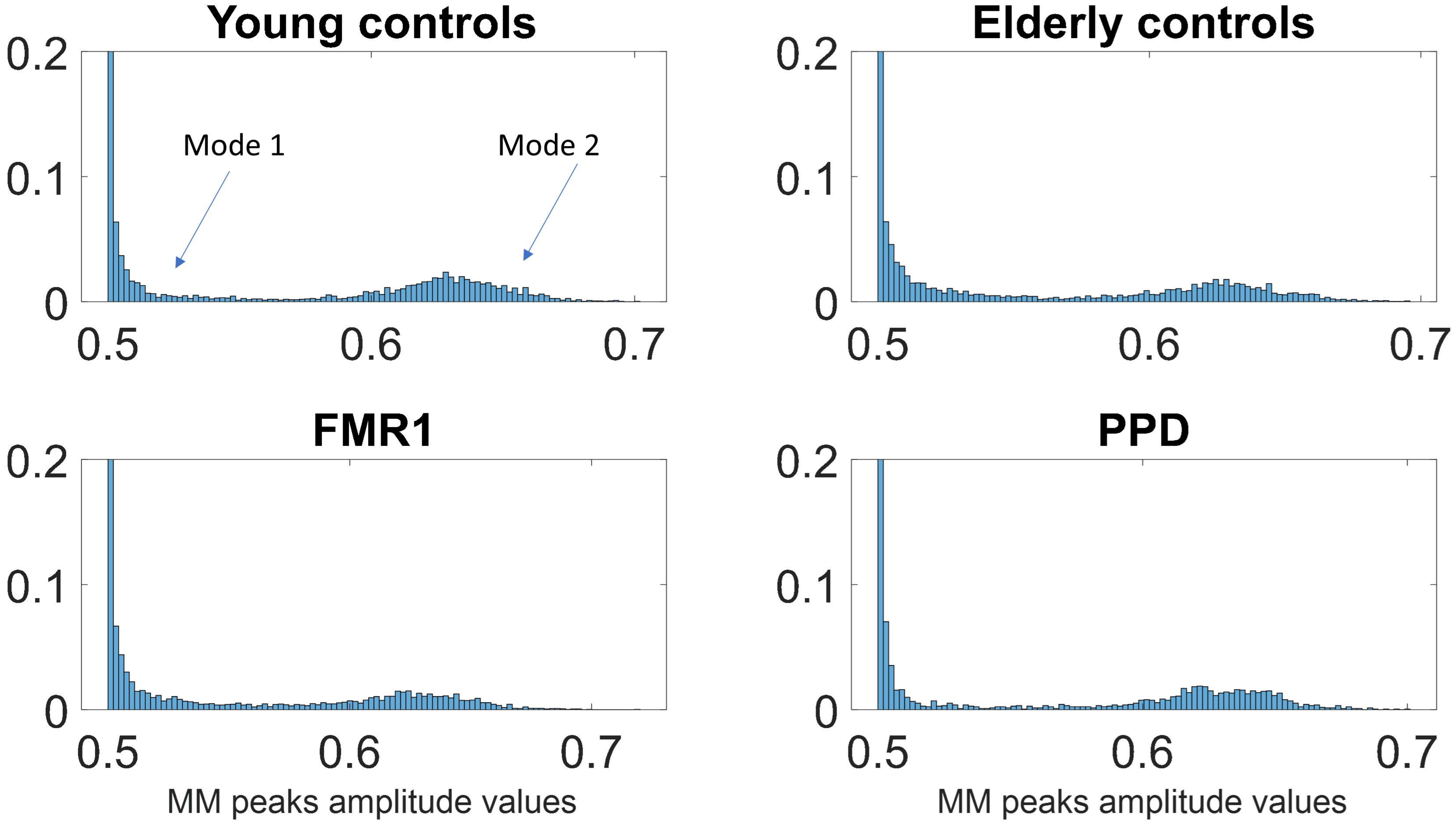
Young controls
Elderly controls
FMR1
PPD
Mode 1
Mode 2
0.2
0.1
0
0.5
0.6
0.7
MM peaks amplitude values

young ct
38%
62%
elderly ct
40%
60%
Mode 1
Mode 2
FMR1
57%
43%
PPD
57%
43%
exponential distribution
MODE 1
pdf
random variable
0
0.1
0.2
0.3
0.4
0.5
0.6
0.7
0.8
0.9
1
0
0.5
1
1.5
2
2.5
3
3.5
4
4.5
5
normal distribution
MODE 2
pdf
random variable
0
0.05
0.1
0.15
0.2
0.25
0.3
0.35
0.4
-3
-2
-1
0
1
2
3

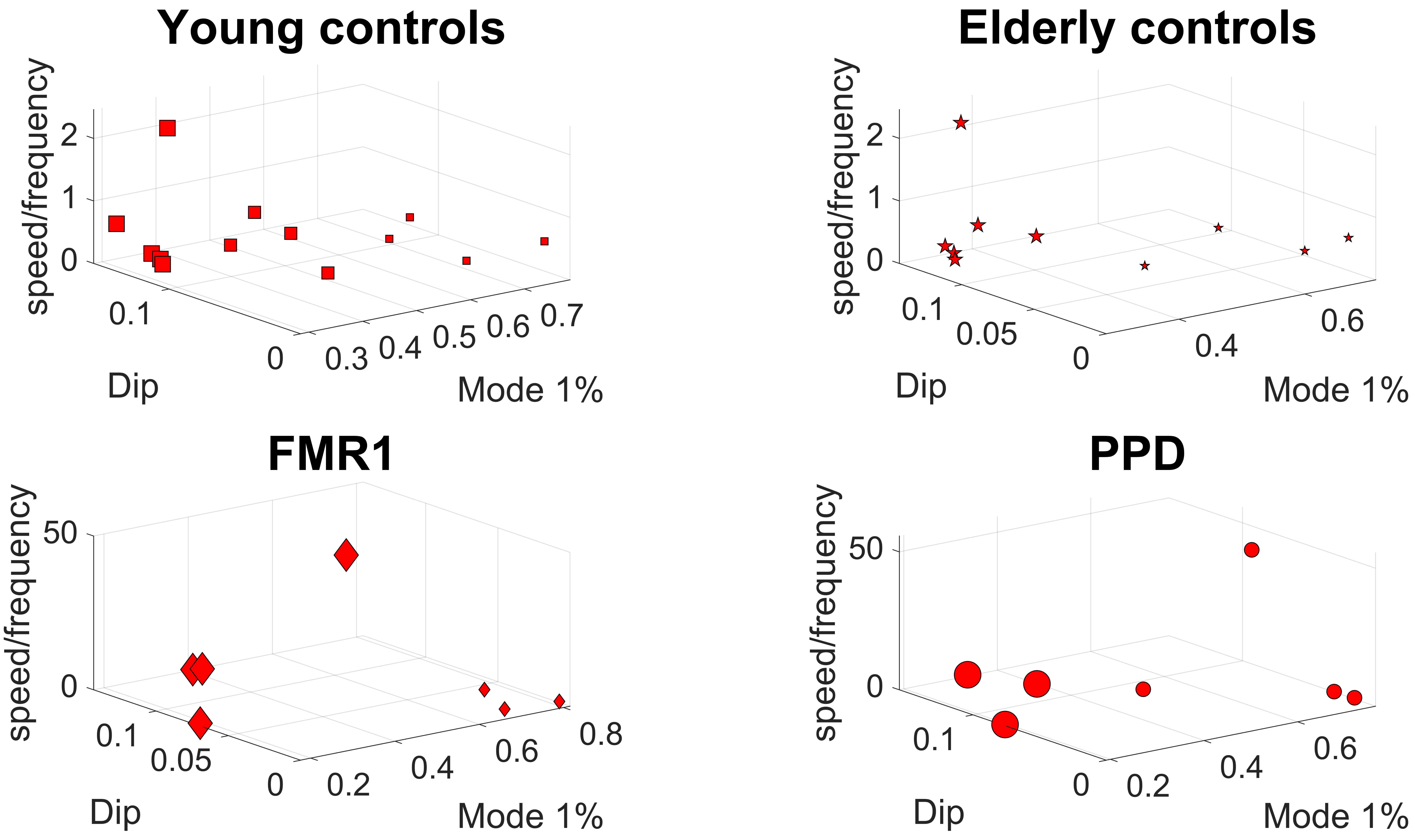
Young controls
speed/frequency
2
1
0
0.1
0
Dip
0.3
0.4
0.5
0.6
0.7
Mode 1%
Elderly controls
speed/frequency
2
1
0
0.1
0.05
0
Dip
0.4
0.6
Mode 1%
FMR1
speed/frequency
50
0
0.1
0.05
0
Dip
0.2
0.4
0.6
0.8
Mode 1%
PPD
speed/frequency
50
0
0.1
0
Dip
0.2
0.4
0.6
Mode 1%

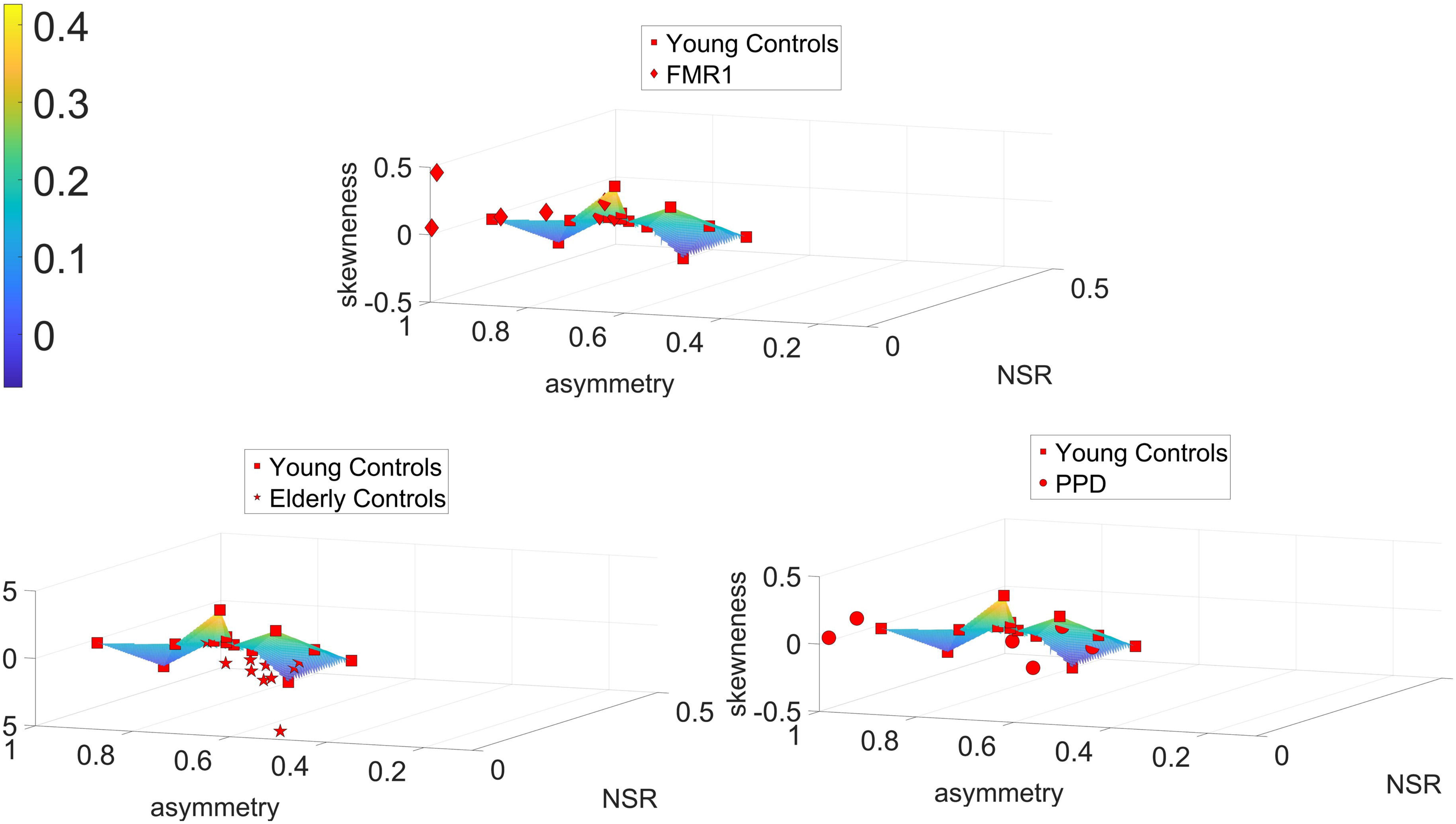
0.4
0.3
0.2
0.1
0
Young Controls
FMR1
skewneness
0.5
0
-0.5
1
0.8
0.6
0.4
0.2
asymmetry
0
0.5
NSR
Young Controls
Elderly Controls
skewneness
0.5
0
-0.5
1
0.8
0.6
0.4
0.2
asymmetry
0
0.5
NSR
Young Controls
PPD
skewneness
0.5
0
-0.5
1
0.8
0.6
0.4
0.2
asymmetry
0
0.5
NSR

Average inter-peak timing differences
Young-Elderly
Young-FMR1
Young-PPD
Elderly-PPD
Elderly-FMR1
FMR1-PPD
Pelvis
L5
L3
T12
T8
Neck
Head
RightShoulder
RightUpperArm
RightForeArm
RightHand
LeftShoulder
LeftUpperArm
LeftForeArm
LeftHand
RightUpperLeg
RightLowerLeg
RightFoot
RightToe
LeftUpperLeg
LeftLowerLeg
LeftFoot
LeftToe
0.04
0.03
0.02
0.01
0
-0.01
-0.02
-0.03

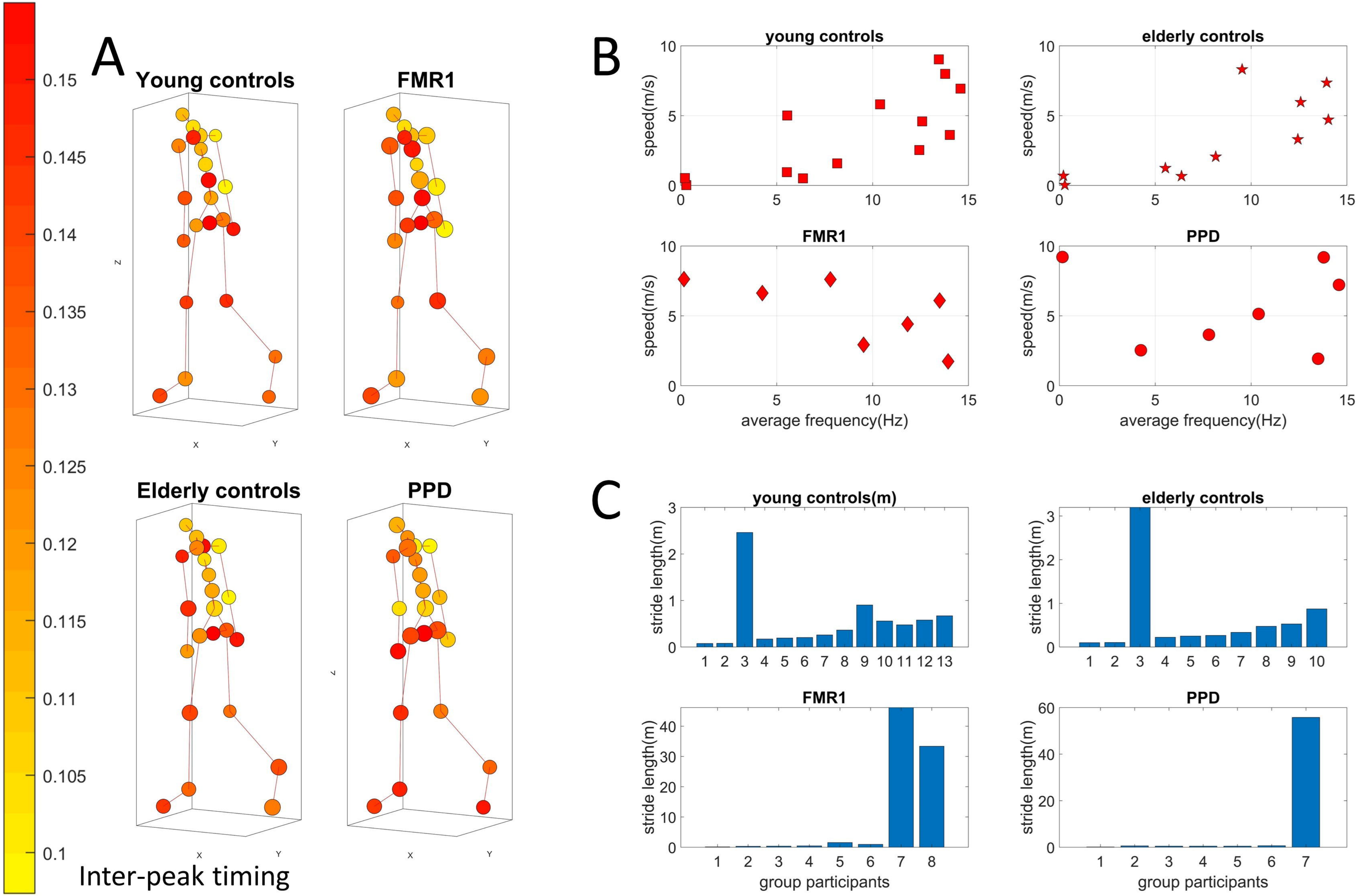
A
Young controls
FMR1
Elderly controls
PPD
X
Y
Z
0.15
0.145
0.14
0.135
0.13
0.125
0.12
0.115
0.11
0.105
0.1
Inter-peak timing
B
young controls
elderly controls
FMR1
PPD
speed(m/s)
average frequency(Hz)
0
5
10
15
C
young controls(m)
elderly controls
FMR1
PPD
stride length(m)
group participants
1 2 3 4 5 6 7 8 9 10 11 12 13
0
1
2
3
10
20
30
40
60

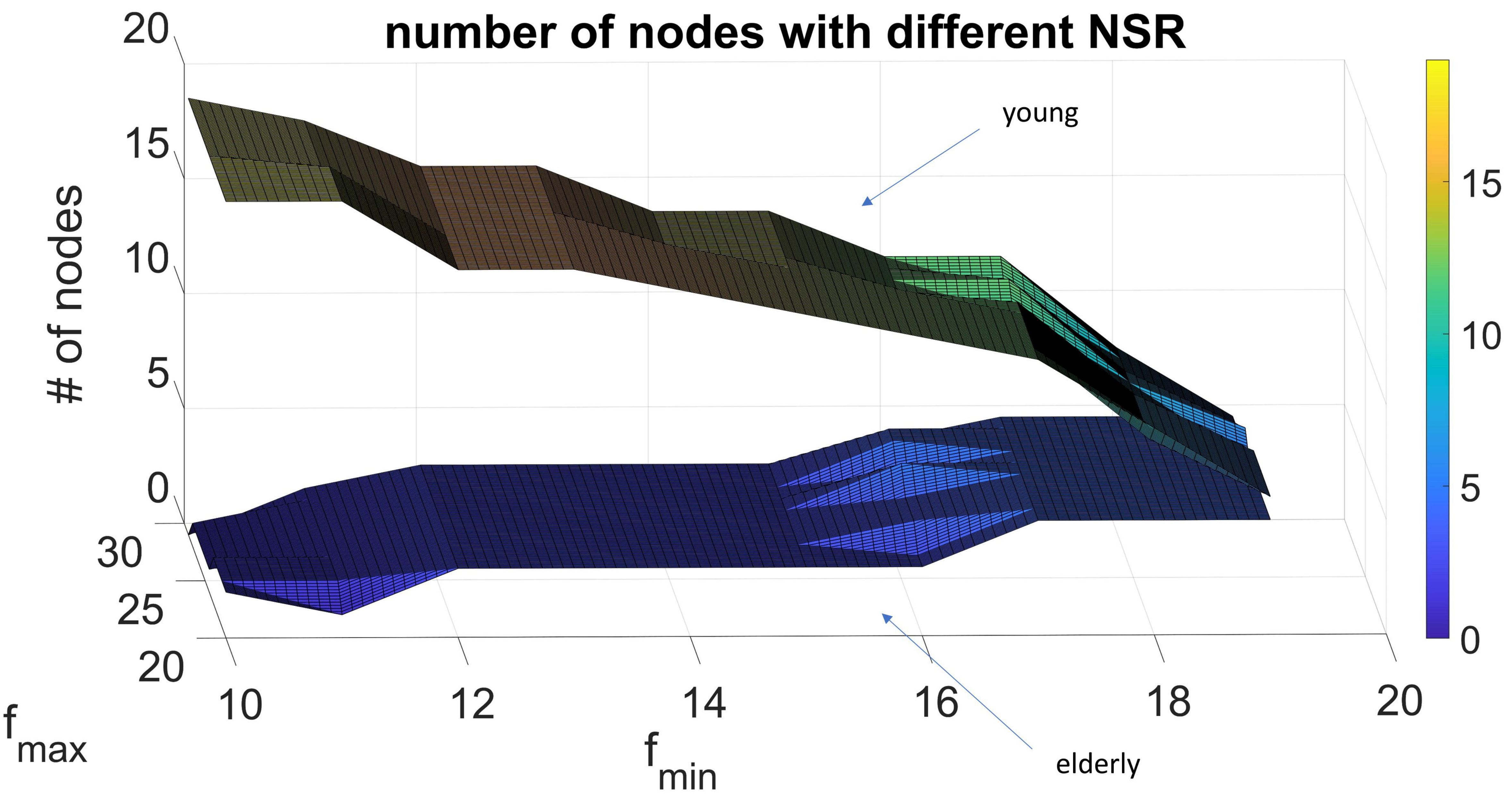
number of nodes with different NSR

young

elderly

young controls
0.5
0
0.5
0.6
0.7
MM peaks
0
5
10
inter-peak intervals
FMR1
0.5
0
0.5
0.6
0.7
MM peaks
0
10
inter-peak intervals
elderly controls
0.5
0
0.5
0.6
MM peaks
0
5
10
inter-peak intervals
PPD
0.5
0
0.5
0.6
0.7
MM peaks
0
10
inter-peak intervals

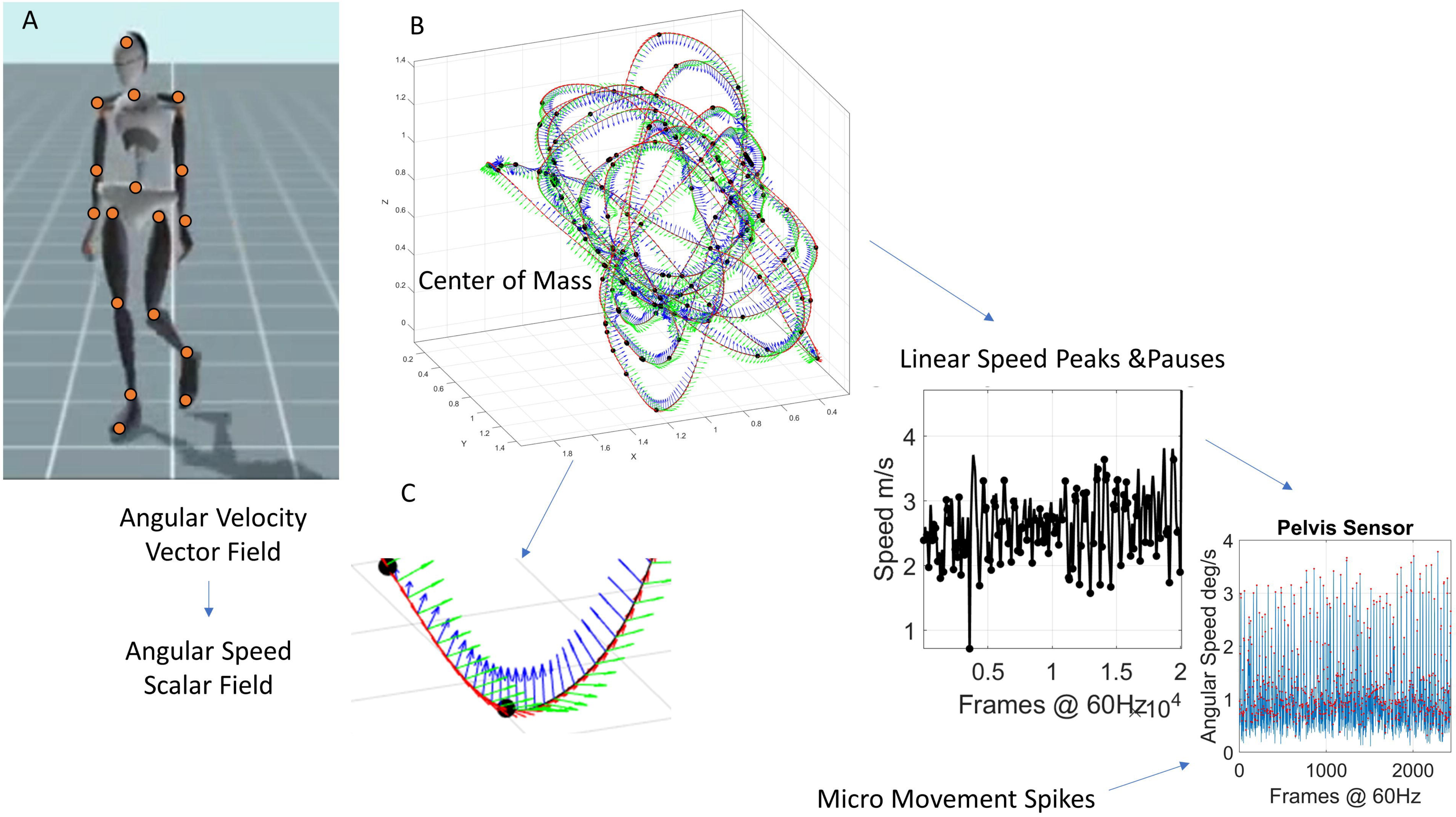
A
B
C
Center of Mass
Z
1.4
1.2
1
0.8
0.6
0.4
0.2
0
Y
0.2
0.4
0.6
0.8
1
1.2
1.4
X
1.8
1.6
1.4
1.2
1
0.8
0.6
0.4
Speed m/s
4
3
2
1
0.5
1
1.5
2
Frames @ 60Hz
×10^4
Pelvis Sensor
Angular Speed deg/s
4
3
2
1
0
0
1000
2000
Frames @ 60Hz

Angular Velocity
Vector Field

Angular Speed
Scalar Field

Linear Speed Peaks &Pauses

Micro Movement Spikes

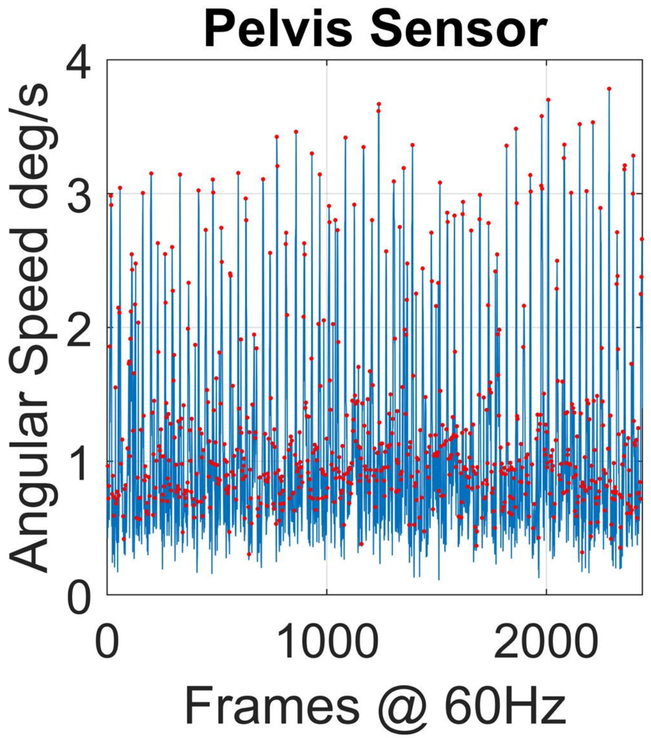

$$NpeakV = \frac{peakV}{peakV + avrgV_{local\ \min\ -to-local\ \min}}$$

Normalize the velocity peaks by the local average

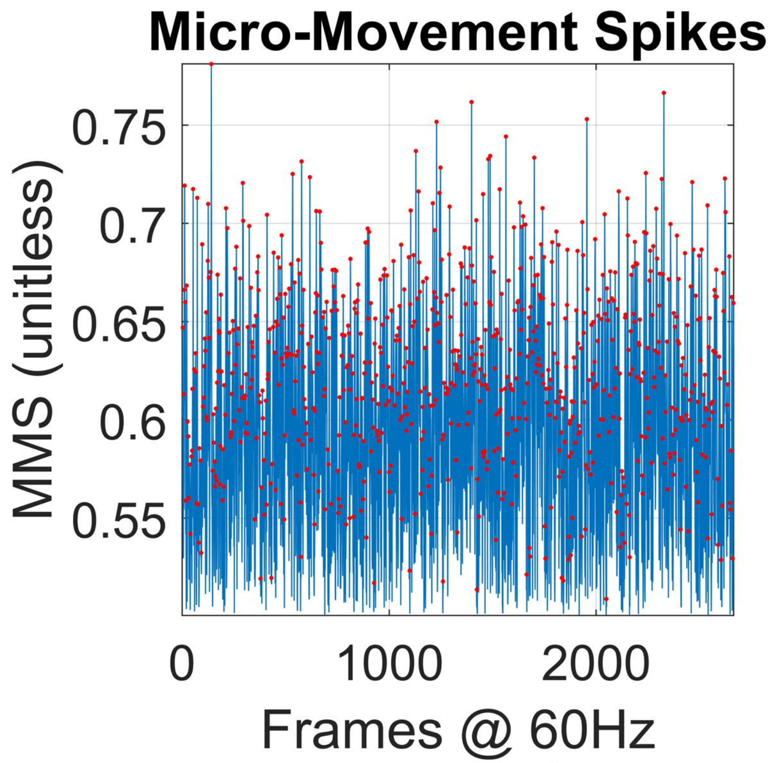

Scaling for Allometric Effects

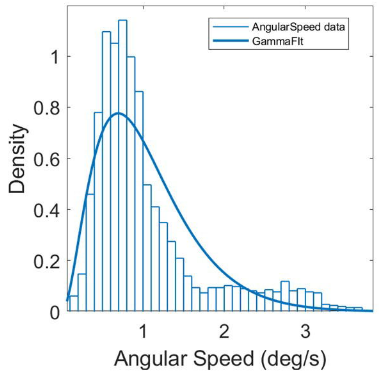

MLE
empirical distributions

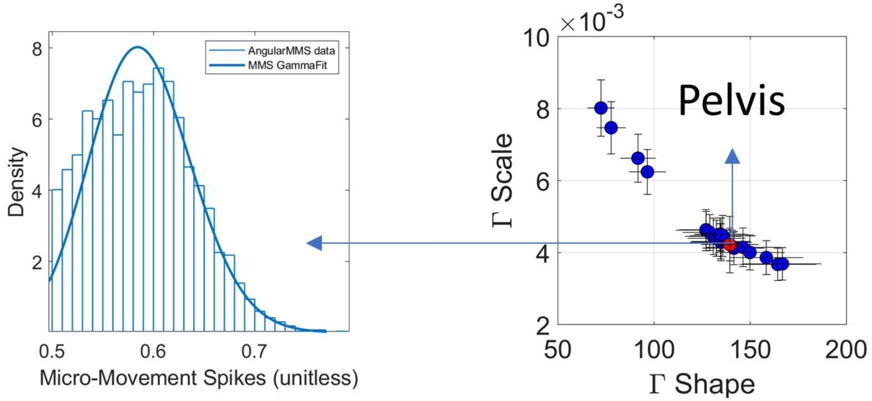

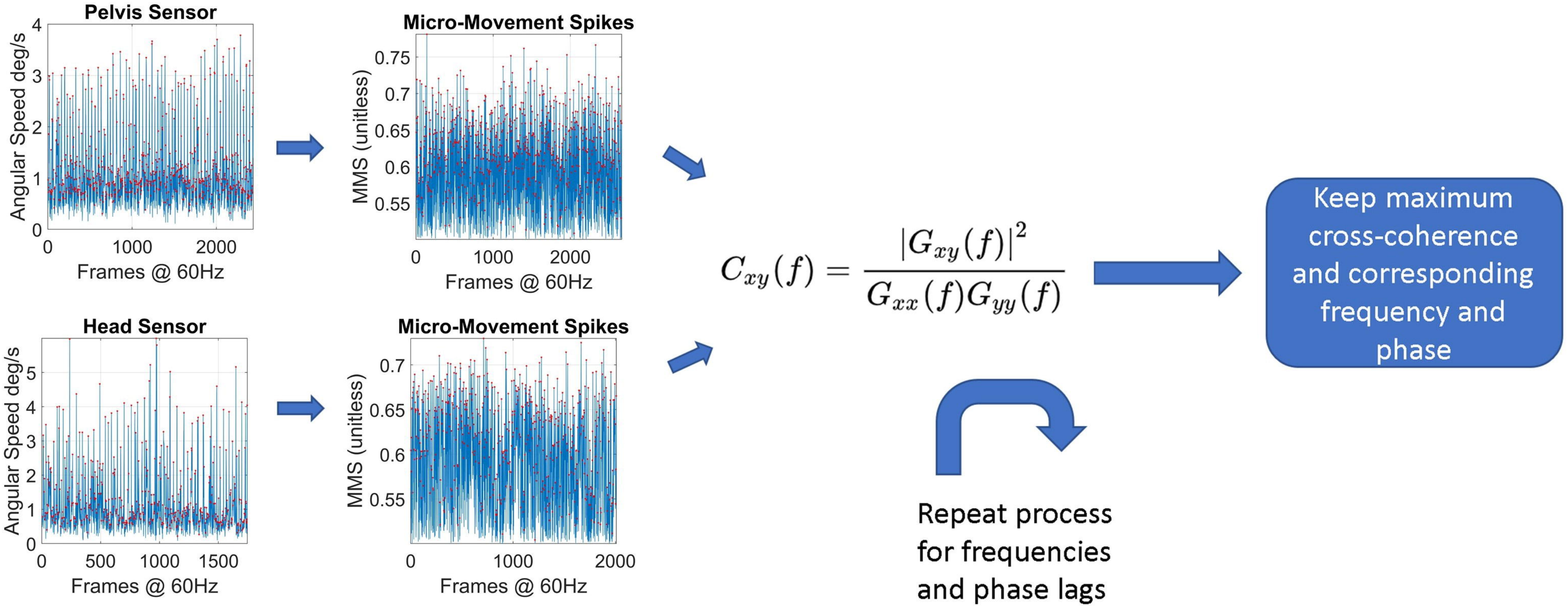
Pelvis Sensor
Angular Speed deg/s
0
1
2
3
4
0
1000
2000
Frames @ 60Hz
Micro-Movement Spikes
MMS (unitless)
0.55
0.6
0.65
0.7
0.75
0
1000
2000
Frames @ 60Hz
Head Sensor
Angular Speed deg/s
0
1
2
3
4
5
0
500
1000
1500
Frames @ 60Hz
Micro-Movement Spikes
MMS (unitless)
0.55
0.6
0.65
0.7
0
1000
2000
Frames @ 60Hz

$$C_{xy}(f) = \frac{|G_{xy}(f)|^2}{G_{xx}(f)G_{yy}(f)}$$

Keep maximum cross-coherence and corresponding frequency and phase

Repeat process for frequencies and phase lags